Bulk Hydrometeor Classification and Quantification Using Polarimetric Radar Data: Synthesis of Relations

JERRY M. STRAKA

School of Meteorology and Center for Analysis and Prediction of Storms, University of Oklahoma, Norman, Oklahoma

DUSAN S. ZRNIĆ

National Severe Storms Laboratory, Norman, Oklahoma

ALEXANDER V. RYZHKOV

Cooperative Institute for Mesoscale Meteorological Studies, University of Oklahoma, and National Severe Storms Laboratory, Norman, Oklahoma

(Manuscript received 18 February 1999, in final form 16 September 1999)

ABSTRACT

A new synthesis of information forming the foundation for rule-based systems to deduce dominant bulk hydrometeor types and amounts using polarimetric radar data is presented. The information is valid for a 10-cm wavelength and consists of relations that are based on an extensive list of previous and recent observational and modeling studies of polarimetric signatures of hydrometeors. The relations are expressed as boundaries and thresholds in a space of polarimetric radar variables. Thus, the foundation is laid out for identification of hydrometeor types (species), estimation of characteristics of hydrometeor species (size, concentrations, etc.), and quantification of bulk hydrometeor contents (amounts). A fuzzy classification algorithm that builds upon this foundation will be discussed in a forthcoming paper.

1. Introduction

The purpose of this paper is to provide a new synthesis of relevant information to deduce dominant or bulk[1] hydrometeor types and bulk amounts from polarimetric radar (PR) data. Thus, the paper lays a foundation for developing semiempirical, rule-based algorithms to deduce dominant hydrometeor types and bulk amounts automatically with computers. The information presented includes PR capabilities, basic hydrometeor characteristics, and PR data signatures necessary for hydrometeor discrimination and quantification. A fuzzy classification algorithm that builds upon this foundation will be discussed in a forthcoming paper.

Some past reviews of PR data interpretations include those by Hall et al. (1984), Herzegh and Jameson (1992), and Doviak and Zrnić (1993). Soon, it will be almost a decade since a comprehensive compilation and synthesis of hydrometeor identification and quantification from PR data at a 10-cm wavelength has been presented. Much has been learned to update and enhance the work done between the 1980s and the early 1990s. Recently, Illingworth and Zrnić (1995), Zrnić (1996), Meischner et al. (1997), and Zrnić and Ryzhkov (1999) have highlighted the increased use of PR for research, and soon there will be a prototype Weather Surveillance Radar 1988 Doppler (WSR-88D) PR (Zrnić 1996; Zahrai and Zrnić 1997; Doviak et al. 2000). The prospects for PR modification on at least some operational WSR-88Ds in the coming decade will expose many in the community to this type of radar and its capabilities. This increase in exposure and growing research use of these radars motivates us to provide a solid presentation, balancing engineering and meteorological aspects of PR use and precipitation physics interpretations, in a single paper. In preparing this paper, so that it, we hope, would

Corresponding author address: Dr. Dusan S. Zrnić, National Severe Storms Laboratory, 1313 Halley Circle, Norman, OK 73069.
E-mail: zrnic@nssl.noaa.gov

[1] All discussion herein about hydrometeor classification with PR refers to bulk hydrometeor identification or identification of the hydrometeor type that dominates the various PR signatures in a radar volume. A word of caution: it is possible, because of physical attributes of a hydrometeor type such as particle structure, density, etc., that relatively few in number of one hydrometeor type (e.g., a few, low-density snow aggregates) might dominate PR signatures in a radar volume even when there are large numbers of another type in the same volume (e.g., many small needle and column crystals).

remain relevant for some time and be complete enough for use by scientists with varying backgrounds, the topics in this synthesis necessarily include descriptions of essentially all of the useful PR variables, physical attributes of the hydrometeor types that permit them to produce signatures detectable by PR, and values of the PR signatures that are associated with the various types of hydrometeors. Many past and recent references are provided to trace the roots of some issues that cannot be covered because of space limitations. Last, because of the deep cross-disciplinary aspects of this topic and our goal to address a multidisciplinary audience, the paper necessarily is extensive. We hope that this extensiveness will enhance its usefulness as a comprehensive synthesis article.

Some of the difficulties in developing procedures to deduce dominant hydrometeor types and bulk amounts from PR data are caused by 1) the lack of a thorough understanding of radar signatures of specific hydrometeor types, 2) the need for information about size distributions and characteristics of hydrometeors, 3) the ambiguities in hydrometeor identifications (several hydrometeor types identified or no type identified), 4) the need for complete sets of quantitative and qualitative observations for rigorous validation, and 5) the occurrence of artifacts in the data and uncertainties in radar calibration. Nevertheless, significant insights already have been obtained concerning the evolution of hydrometeors in convective storms (e.g., Wakimoto and Bringi 1988; Tuttle et al. 1989; Bringi et al. 1991; Fulton and Heymsfield 1991; Herzegh and Jameson 1992; Holler et al. 1994; Bringi et al. 1996; Jameson et al. 1996; Straka 1996; Bringi et al. 1997; Lopez and Aubagnac 1997; Meischner et al. 1997; Carey and Rutledge 1998; Hubbert et al. 1998) and stratiform precipitation events (e.g., Herzegh and Jameson 1992; Zrnić et al. 1993a; Ryzhkov and Zrnić 1998a). In addition, there is promise that PR measurements might help to improve quantitative estimates of liquid and solid forms of precipitation (e.g., Seliga and Bringi 1976; Sachidananda and Zrnić 1986, 1987; Aydin et al. 1990; Balakrishnan and Zrnić 1990a; Chandrasekar et al. 1990; Aydin et al. 1995; Ryzhkov and Zrnić 1995a,b, 1996a,b; Zrnić and Ryzhkov 1996; Ryzhkov and Zrnić 1998a,c; Ryzhkov et al. 1998). So far, there have been few, though apparently successful, attempts to describe the bulk hydrometeor distributions, primarily in convective cloud systems with PR data using physical and semiempirical rules (e.g., Hall et al. 1984; Zrnić et al. 1993b; Holler et al. 1994; Straka 1996; Lohmeier et al. 1997; Lopez and Aubagnac 1997; Meischner et al. 1997).

There are a number of scientific and operational reasons for attempting to develop algorithms to deduce hydrometeor types and amounts from PR data. These include 1) calibration of precipitation rates from nonpolarimetric radars such as WSR-88D (Next-Generation Radar), 2) determination of interactions between microphysics and kinematics in severe storms and mesoscale systems, 3) estimation of latent heating for global energy budgets by discriminating between ice and liquid precipitation using spaceborne PR radars, 4) evaluation of advertent and inadvertent weather modification, 5) investigation of lightning production in deep convective clouds, 6) initialization of hydrometeor types and amounts in storm-scale and mesoscale numerical models, 7) determination of detrainment rates in hybrid-cumulus parameterization schemes (e.g., Frank and Cohen 1987; Straka 1994), 8) improvement and verification of microphysical parameterizations in cloud and mesoscale models (Straka 1996), and 9) verification of quantitative precipitation forecasts (Fritsch et al. 1998), among others.

In section 2, we begin by reviewing some of the observed and computed PR variables. Next, we describe hydrometeor characteristics as they are relevant to PR discrimination and justify the use of various PR variables to identify hydrometeor types in section 3. When presented information about hydrometeor types, logical questions a scientist might ask are: ''What is the evidence?,'' ''What are the limitations of the information?,'' and ''What is the amount?'' The former two questions justify the need for sections 2 and 3, whereas the latter question justifies the need for section 4, in which we present methods for precipitation characterization and amount quantification. To provide complete and critical answers to the question, ''What are the limitations of the information?'' for all of the information presented in this paper would be a very difficult and arduous task at this time because of limited in situ data to compare with theoretical calculations, scattering-model results, and PR data. Nevertheless, the question is of the utmost importance to consider when using PR data for meaningful studies of cloud and precipitation physics. It is suggested that the reader might address these questions and similar ones on a case-by-case basis by reviewing articles cited herein. Estimation errors are not reviewed either; they can be obtained from simulations (Galati and Pavan 1995) or analytic formulas (Ryzhkov and Zrnić 1998c). Last, this paper is closed with a short summary in section 5.

The basis of our hydrometeor classification and quantification algorithm, described in detail along with examples in a forthcoming paper, is fuzzy characterization or fuzzy logic [see Mendel (1995) for a review]. A brief description of the algorithm aimed at a broad audience is in a recent *Bulletin of the American Meteorological Society* article (Vivekanandan et al. 1999), and, in the same volume, there is an example of classification in a severe hail storm (Zrnić and Ryzhkov 1999). The information provided herein also might be useful for construction of other types of rule-based algorithms.

2. Polarimetric radar variables

Several of the PR variables have been obtained with radars in the United States such as the Cimarron radar

in Oklahoma (Zahrai and Zrnić 1993), the Phillips Laboratory (successor to the Air Force Geophysics Laboratory) radar in Sudbury, Massachusetts (Metcalf et al. 1993), the National Center for Atmospheric Research S-band Doppler dual-polarization radar (S-POL) in Colorado, or the Colorado State University–University of Chicago and Illinois State Water Survey (CSU-CHILL) radar in Colorado (Bringi et al. 1993). Polarimetric radar measurements also are available from European (e.g., Schroth et al. 1988; Meischner et al. 1997; Blackman and Illingworth 1993), Japanese (e.g., Uyeda et al. 1991), Australian (May et al. 1999b; Keenan et al. 1998), and other radars.

We consider dual, linear switchable polarization systems with reception of both copolar and cross-polar components. There are two fundamental kinds of variables available from dual, linear polarization radars. Intrinsic variables provide information about backscatter from hydrometeors in a resolution volume; herein, it is assumed that these variables are not biased by propagation effects (i.e., attenuation and cross coupling). Propagation variables provide information about hydrometeors between the radar and a resolution volume. These variables can be combined to obtain information about dominant, bulk hydrometeor types and amounts both in a resolution volume and between the radar and a resolution volume. Moreover, combining them provides a powerful means for building sets of relations for bulk hydrometeor classification. Basic equations for the most commonly used PR variables are listed in appendix A. An analytical discussion of these variables and others (not used herein) is presented by Zrnić (1991) and Doviak and Zrnić (1993), both of which provide many references. Examples of polarimetric data fields, including signatures of weather events and biological scatterers, are presented by Zrnić and Ryzhkov (1999). A brief, qualitative description of the known useful variables follows as they pertain to hydrometeor identification and quantification. In the rest of this paper, all discussion applies to a 10-cm wavelength radar at quasi-horizontal (elevation angle less than 30°) incidence (except where indicated).

a. Reflectivity

Reflectivity factors for horizontally and vertically polarized waves Z_h and Z_v [Eqs. (A1–A2)] are proportional to the hydrometeor's cross section integrated over a volume. For a particle of given size, ice produces lower Z_h and Z_v than does liquid because of lower dielectric effects; the dielectric constant is about 20% that of liquid for high-density ice and can be less than 5% that of liquid for low-density ice (function of size and density of ice—lower-density ice can be associated with lower dielectric effects). It is important to recognize that Z_h and Z_v are sensitive to calibration, and, even at 10 cm, wavelength can be affected by attenuation in heavy precipitation (Ryzhkov and Zrnić 1995c). The variables Z_h and Z_v together, and combined with other PR variables, are very useful to discriminate hydrometeor types (e.g., Aydin et al. 1986a,b; Leitao and Watson 1984; Golestani et al. 1989; Balakrishnan and Zrnić 1990a,b; Walsh 1993; and Ryzhkov and Zrnić 1998a; as described next).

b. Differential reflectivity

Differential reflectivity Z_{dr} [Eq. (A3)], which is obtained from the ratio of Z_h and Z_v, can be related to the axis ratio and size of hydrometeors (e.g., Seliga and Bringi 1976; axis ratio is defined as a/b, where a is the horizontal axis radius, and b is the vertical axis radius). To be more specific, Z_{dr} is a measure of the reflectivity-weighted mean axis ratio of hydrometeors in a volume. For scatterers that are small in comparison with the radar wavelength (Rayleigh conditions) and oriented with their symmetry axis vertical in the plane of polarization, axis ratios less than unity produce positive Z_{dr}. Conversely, axis ratios larger than unity produce negative Z_{dr}. Canting affects Z_{dr} because of changes in effective lengths of the scatterers along the directions of orthogonal polarized transmitted electric fields. Numerous larger-size hydrometeors can strongly influence Z_{dr} signals because they produce large reflectivities. The dielectric constant affects Z_{dr} much less if the hydrometeors are ice than if they are composed of or are coated by liquid. Differential reflectivity is independent of calibration and total concentration but can depend on how the concentration is distributed among various sizes. Also, differential reflectivity is not immune to propagation effects.

c. Reflectivity difference

In addition to Z_{dr}, the reflectivity difference Z_{dp} [Eq. (A4)] is another convenient combination of Z_h and Z_v. Unlike Z_{dr}, because Z_{dp} is obtained from the difference of Z_h and Z_v, it depends on hydrometeor concentration and can be used to compute the ice and liquid contributions to Z_h from a rain and ice mixture (Golestani et al. 1989; Tong et al. 1998). Golestani et al. (1989) showed that Z_{dp} indicates the anisotropy (mean apparent shape tends toward oblate or prolate spheroids) of the shapes of hydrometeors; nonspherical, oriented hydrometeors produce different Z_h and Z_v, and, in the difference, the contribution from statistically isotropic (mean apparent shape tends toward a sphere) hydrometeors vanishes.

d. Differential phase and specific differential phase

The differential phase ϕ_{dp} [Eq. (A5)] is the only propagation variable that is easy to measure and to use. In a volume filled with horizontally oriented hydrometeors such as rain or ice crystals, a horizontally polarized wave has larger phase shifts (per unit length) and propagates more slowly than a vertically polarized wave

does; the opposite holds for vertically oriented hydrometeors. The specific differential phase K_{dp} [Eq. (A6)] is the difference between propagation constants for horizontally and vertically polarized waves (k_{hh} and k_{vv}). In theory, K_{dp} allows discrimination between statistically isotropic and anisotropic hydrometeors; isotropic hydrometeors produce similar phase shifts for horizontally and vertically polarized waves. Therefore, differences are due to anisotropic constituents. In general, the magnitude of K_{dp} increases as both oblateness (or prolateness) and dielectric constant increase. The advantages of using K_{dp} to estimate precipitation rates of anisotropic hydrometeors (Zrnić and Ryzhkov 1996) include that it is 1) independent of receiver/transmitter calibration, 2) independent of attenuation, 3) less sensitive than Z_h or Z_v are to variations of size distributions, 4) immune to partial beam blockage, and 5) not biased by the presence of statistically isotropic hydrometeors such as randomly oriented hail. The effects of reflectivity gradients within the beam affect K_{dp} more than they do other polarimetric variables (Ryzhkov and Zrnić 1998b), and a method to identify these gradients needs to be developed. Specific differential phase also is dependent on hydrometeor number concentration.

e. Backscatter differential phase

In the absence of propagation effects, the backscatter differential phase δ is obtained from the argument of the correlation coefficient $|\rho_{hv}(0)|$ (Doviak and Zrnić 1993), which is defined next. In general, nonzero values of δ can indicate resonance scattering [scattering beyond the Rayleigh regime (McCormick et al. 1979; Doviak and Zrnić 1993)] by partially aligned hydrometeors. Aydin and Giridhar (1992) show that hydrometeors larger than one-tenth the radar wavelength can produce a sharp δ discontinuity. In the resonance regime, ϕ_{dp} contains contributions from the backscatter differential phase δ that can be estimated by filtering ϕ_{dp} data along range (Hubbert and Bringi 1995). For resonance regime scatterers, δ can depend on the size of nonspherical hydrometeors. Modeling of a hydrometeor's backscatter demonstrates that there is a change in the sign of δ over narrow ranges of particle sizes (Balakrishnan and Zrnić 1990b). As a result, it is hypothesized that δ could be used to interpret the size and type of nonspherical hydrometeors (Zrnić et al. 1993a). At a 10-cm wavelength, smaller particles (diameter $D < 10$ mm) generally should not produce significant δ.

f. Correlation coefficient

The degree of decorrelation as measured using the correlation coefficient at zero lag $|\rho_{hv}(0)|$ [Eq. (A7)] between horizontally and vertically polarized echoes results, for Rayleigh scatterers, from variability in the horizontal and vertical sizes of hydrometeors. This relation is because the backscatter intensity for the Rayleigh scattering depends monotonically on the dimension of hydrometeors in the direction of the electric field. Use of $|\rho_{hv}(0)|$ is much more complicated for resonance-regime scatterers, because then backscatter differential phase shift is not zero. Decorrelation physically occurs if the horizontal and vertical backscatter fields do not vary similarly. This situation might occur when changes in the horizontal and vertical backscatter fields, caused by each particle in a resolution volume, are not proportional to each other and the particles reorient and/or when there is a change in the number of particles. In support of this reasoning, modeling and observation studies show that $|\rho_{hv}(0)|$ decreases with increasing diversity of hydrometeor orientations and shapes (e.g., Jameson 1989; Balakrishnan and Zrnić 1990b; and (Zrnić et al. 1993a). Decorrelation also can be more significant when particles are wet or when they are large and irregular in shape. Moreover, $|\rho_{hv}(0)|$ is lower when there are mixtures of hydrometeor types rather than when just one type is present (Jameson 1989). The lowest values of $|\rho_{hv}(0)|$ theoretically should occur when there are mixtures of equal amounts of two different types, especially when the size of one varies predominantly in the horizontal and the other varies in the vertical direction. Values of $|\rho_{hv}(0)|$ are independent of radar calibration and hydrometeor concentration. In addition, $|\rho_{hv}(0)|$ is immune to propagation effects.

g. Linear depolarization ratio

The linear depolarization ratio LDR_{vh} [Eq. (A8)] is the logarithm of the ratio of the cross-polar power received to the copolar power received. For a horizontally polarized transmitted wave, a spherically shaped hydrometeor would reflect a likewise (horizontally) polarized wave, resulting in LDR_{vh} equal to $-\infty$ dB. The same applies to axially symmetric particles for which the axis of symmetry is vertical or horizontal in the polarization plane; otherwise, there would be cross-polar power returned. The hydrometeor characteristics associated with depolarization of transmitted energy include hydrometeor shape, shape irregularity, thermodynamic phase, dielectric constant, and canting in the plane of polarization (Herzegh and Jameson 1992). In addition, randomly oriented symmetric particles produce a minimum in $|\rho_{hv}(0)|$, which is related to LDR_{vh} by $|\rho_{hv}(0)|_{\min} = 1\text{–}2 \times 10^{(0.1\mathrm{LDR}_{hv})}$ (Jameson 1989; Mead et al. 1991; Hubbert et al. 1998). In general, LDR_{vh} tends to be more susceptible to noise than other PR variables such as Z_{dr}, because the cross-polar signal is typically two to three orders of magnitude smaller than the copolar signal. From a practical point, though, the lowest observable value for LDR_{vh} with, for example, the S-POL radar is about -30 dB (determined by the authors from examinations of the S-POL data collected in 1998 in Florida). With the CSU-CHILL radar, the lowest possible LDR_{vh} is about -34 dB (Hubbert et al. 1998). LDR_{vh} is independent of number concentration

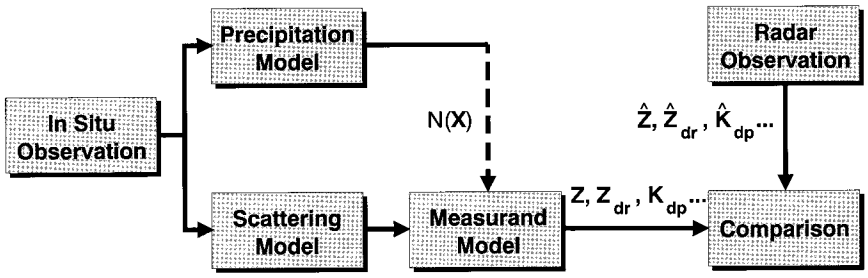

FIG. 1. Schematic of hydrometeor discrimination philosophy. Note the linkages among the in situ observation, precipitation model, scattering model, and measurand model for comparing radar observations with actual observations of hydrometeors: $\mathbf{N}(X)$ represents concentrations of hydrometeors and includes their characteristics (i.e., shape, canting angle, dielectric constant); Z, Z_{dr}, and K_{dp} (among others) are polarimetric variables from models; $\hat{Z}$, $\hat{Z}_{dr}$, and $\hat{K}_{dp}$ are polarimetric variables from observations.

and radar calibration. LDR_{vh} unfortunately is not immune to propagation effects. There is no quantitative information about precipitation amounts available from LDR_{vh}. Because most previous use of LDR_{vh} has been with 3-cm-or-shorter-wavelength radar, there are few comparisons between 10-cm-wavelength LDR_{vh} values and in situ observations. Exceptions include observations and modeling studies by Frost et al. (1989, 1991) for various basic types of hydrometeors [see Fig. 8.29 in Doviak and Zrnić (1993)]. Also, Vivekanandan et al. (1994) have modeled LDR_{vh} for various hydrometeors at 10-cm wavelength. More recently, Carey and Rutledge (1998) and Hubbert et al. (1998) have presented comparisons between LDR_{vh} signatures obtained with the CSU-CHILL radar and hydrometeor observations made at the ground.

3. Classification

Identification of hydrometeor types using PR data is accomplished by associating different bulk hydrometeor characteristics with the unions of subsets of values of the various PR variables. In principle, several methods are available to achieve this goal. The classic approach is the statistical decision theory whereby regions in the PR variable space are sought such that the probability of correct classification is maximized for a given probability of a wrong classification. This approach requires statistical information that is not yet available. Another method, based on neural networks, also could be devised. Although powerful, this method needs a verified training set of considerable size that currently does not exist. Furthermore, it is unlikely that such a set will become available in the foreseeable future. On the other hand, rule-based methods are not prone to these shortcomings because they are tied to physical principles. Thus, it is possible to evolve the rule-based methods in step with the progress in understanding the physical principles. Consequently, we lay foundations for these methods by partitioning the PR variable spaces into subsets corresponding to specific, bulk hydrometeor types. Partitions of individual variables are presented in tables. Thus, even if only one of the variables is available, a crude classification still can be made. Where there are known relations between pairs of variables, partitions are presented in graphs. Admittedly, these graphs sometimes are difficult to construct such that they all agree exactly with each other at boundaries because of the uncertainties in hydrometeor identification with PR data. Also, inherent statistical errors increase the uncertainty of the boundaries. Therefore, a conservative philosophy in constructing graphs is generally adopted. The titles of the tables refer to the general species or habits of hydrometeors, and the PR variable boundaries of this general class (e.g., rain) are listed in the first row. In subsequent rows, we present the boundaries of subdivisions of the general species of hydrometeors (e.g., small drops, medium drops, and large drops for rain).

Ambiguities in hydrometeor identification with PR data might be reduced, by a yet-to-be-determined amount, by invoking arguments based on physical considerations. Another source of information for identifying hydrometeor types and, possibly, for reducing identification ambiguities comes from self-consistency among the PR variables; if two or more PR variables suggest a certain hydrometeor type, the identification procedure should be more reliable. Much support for understanding hydrometeor scattering properties has come from modeling studies. A brief review of the philosophy behind the use of scattering models, in the framework of observing and simulating PR-variable signatures of hydrometeors, is presented by Aydin and Zrnić (1992). As shown in Fig. 1, precipitation models are used to specify characteristics of hydrometeors such as size distributions, concentrations, shapes, orientations, dielectric constants, and others, which all are contained in the vector $\mathbf{X}$. Scattering models are used to compute the forward-scattering and backscattering amplitudes of individual hydrometeors. The PR variables (e.g., Z_h, Z_{dr}, LDR_{vh}, K_{dp}, ϕ_{dp}, $|\rho_{hv}(0)|$) are computed using the precipitation model (stored in the vector $\mathbf{X}$) and the scattering amplitudes. Results from this stage then are compared with observations for validation. Ex-

planations of the differences between observed and computed PR variables might be used to update the precipitation and scattering models.

Comprehensive in situ measurements of hydrometeor types and amounts to validate PR data are very difficult to obtain. The possible exception to this scarcity is from, perhaps, measurements at the ground (hail size from observing networks and raindrop size distributions from disdrometer measurements). In situ observations of rain, small hail, ice crystals, and graupel are also available from aircraft (Bringi et al. 1986a, 1991; Aydin et al. 1993; Brandes et al. 1995; Bringi et al. 1997; and Ryzhkov et al. 1998; just to name a few). Most aircraft observations, however, are point measurements or along-line measurements with very limited temporal and spatial resolutions. Very promising are comparisons between vertically looking radars and polarimetric radars (May et al. 1999a). In these measurements, the resolution volume sizes are compatible, and Doppler spectra from the vertically looking radars can reveal the distribution of drops, hail, and, perhaps, some ice crystals. This kind of research has just begun and hopes are high that it will provide some clues; still, it is not likely that the comprehensive observations needed fully to validate PR analyses of hydrometeor types and amounts will be available in the near future.

In the remainder of this section, we first present specifics about hydrometeor characteristics (required for modeling and interpreting PR data) and then present relations between the values of PR variables and bulk hydrometeor types. The general hydrometeor types considered are hail, graupel/small hail, rain, and crystals/snow aggregates (snow hereinafter generally refers to aggregates). Also included for classification purposes is temperature T because it can be estimated from a proximity sounding (from which updraft and downdraft temperatures can be crudely determined) or possibly from thermodynamic retrievals (Gal-Chen 1978) when three-dimensional winds can be approximated from multi–Doppler radar data or single-Doppler data (e.g., Shapiro et al. 1995; Sun and Crook 1996). The use of temperature is most important in minimizing some unreasonable ambiguities. For example, ice crystals would not be expected at 15°C, and rain would not be expected at −30°C. There are various ways the boundaries of PR variables and temperature thresholds in the tables and graphs can be applied for hydrometeor type classification. A simple way is to assume the boundaries are rigid and classify according to majority rule; that is, the class that satisfies the thresholds for the most PR variables is declared to be present. Ambiguous signatures also could be specified. Better classifiers can be designed if the boundaries are ''porous''; that is, a hydrometeor type is allowed to exist on either side of a boundary (Straka 1996; Vivekanandan et al. 1999). We adopt this definition: the boundaries presented are ''fuzzy,'' and the confidence of hydrometeor classification at the threshold boundaries is 0.5 on a scale of 0–1. Various functions, such as sigmoid, bell, Gaussian, trapezoid, or triangle can be used to prescribe the confidences in the vicinity of the boundaries, with values ranging between 0.0 and 1.0 (e.g., Straka 1996). It is important to realize that, depending on what is on the other side of the boundary, the relative significance of different segments for a specific hydrometeor type can be very different. For example, a segment of a boundary between rain and hail is much more significant than a segment that delineates rain from a forbidden region (i.e., a region where it is not possible for hydrometeors to produce PR signals). It is important to specify well the former, whereas, for the latter, it suffices to make sure that it encompasses all the PR data corresponding to rain.

a. Hail

Detecting the presence of hail and its size has been a long-standing goal of radar meteorologists. Several physical characteristics of hail help to make it distinguishable from other hydrometeors in PR radar data. Yet, the orientation of hail in fall is not fully understood or documented, so gauging its size would be difficult, as the following discussion amply demonstrates. For example, List (1986) describes at least a weak association between hail size and shape; that is, hail 5–10 mm in diameter is spherical or conical, hail $10 < D < 20$ mm is ellipsoidal or conical, hail $10 < D < 50$ mm is ellipsoidal with lobes and other protuberances along the short axis, and hail $40 < D < 100$ mm is spherical with small and large lobes and other protuberances. List (1986), however, found no simple relation between protuberance size and number and the size of hail, although larger hail tends to be more irregular. Another observation is that most hailstones are oblate to at least some degree (Barge and Isaac 1973); for example, 83% have axis ratios between 0.6 and 1.0, 15% have axis ratios between 0.4 and 0.6, and less than 2% have axis ratios less than 0.4. In addition, the majority of hailstones observed at ground have axis ratios (minor to major) of 0.8 (Knight 1986; Matson and Huggins 1980). Wet hail typically has an axis ratio of about 0.8, and spongy hail has an axis ratio of 0.6 to 0.8 (Knight 1986). The orientation of falling hail is somewhat questionable. There is evidence that hailstones fall with their maximum dimensions in both the horizontal (Knight and Knight 1970; List et al. 1973; Matson and Huggins 1980) and the vertical (Knight and Knight 1970; Kry and List 1974). List (1986) suggested that ellipsoidal hailstones 10–50 mm in diameter typically fall most stably when oriented in the vertical, which is in agreement with frequent observations by one of the authors of this paper (J. M. Straka). Hailstones also can exhibit gyrating motions (List et al. 1973; Kry and List 1974) and tumbling motions (List et al. 1973; Knight and Knight 1970; Matson and Huggins 1980). Tumbling hail may have an apparent axis ratio of unity; that is, it may appear statistically to be spherical or isotropic. The structure of

TABLE 1. Equations and parameters for hail.

Parameter	Equations	References
Distribution	$n(D) = n_o \exp(-D\lambda)$ (m^{-4}) exponential distribution $n(D) = n_o D^{\mu} \exp(-D\lambda)$ (m^{-4}) gamma distribution $n(D) = aD^b$ (m^{-4}) power law distribution [D (m), $a = 3.5416 \times 10^{-5}$, and $b = -3.4$]	Lin et al. (1983), Cheng and English (1983), Ulbrich and Atlas (1982), Ferrier (1994), and Pruppacher and Klett (1981)
Total number	$N_t = n_o \lambda^{-1}$ (m^{-3}) exponential distribution $N_t = n_o \lambda^{-(1+\mu)} \Gamma(1 + \mu)$ (m^{-3}) gamma distribution	Lin et al. (1983) and Ferrier (1994)
Slope*	$\lambda = [(\rho n_o \pi)/(\rho_{air} q)]^{-1/4}$ (m^{-1}) exponential distribution $\lambda = (2.3 \times 10^6/Z_h)^{-3.37}$ (m^{-1}) exponential distribution $\lambda = \{[\Gamma(4 + \mu)\rho N_t \pi]/[6\Gamma(1 + \mu)\rho_{air} q]\}^{-1/3}$ (m^{-1}) gamma distribution	Lin et al. (1983), Cheng and English (1983), Doviak and Zrnić (1993), and Ferrier (1994)
Intercept	$n_o = 4 \times 10^4$ (m^{-4}) exponential distribution $n_o = 115 \times 10^3 \lambda^{3.63}$ (m^{-4}) exponential distribution $n_o = N_t \lambda^{-(1+\mu)}[\Gamma(1 + \mu)]^{-1}$ ($m^{-(4+\mu)}$) gamma distribution	Lin et al. (1983), Cheng and English (1983), Doviak and Zrnić (1993), and Ferrier (1994)
Median diam (D_o) and mass-weighted mean diam (D_m)	$D_o = 3.67\lambda^{-1}$ (m); $D_m = 4\lambda^{-1}$ (m) exponential distribution $D_o = (3.67 + \mu)\lambda^{-1}$ (m); $D_m = [\Gamma(5 + \mu)/\Gamma(4 + \mu)]\lambda^{-1}$ (m) gamma distribution	Doviak and Zrnić (1993)
Density	$\rho = 900$ (kg m^{-3}) Note that hail density can vary though larger hail (>20 mm) is usually high density	Pruppacher and Klett (1981)
Fall velocity*	$V = [(4\rho Dg)/(3\rho_{air} C_d)]^{0.5}$ (m s^{-1}) ($0.45 < C_d < 0.60$) $V = 3.95 Z_h^{0.148}$ (m s^{-1})	Pruppacher and Klett (1981) and Conway and Zrnić (1993)
Shape	Sphere ($a/b = 1.0$; $D < 10$ mm) Ellipse ($a/b = 0.9$; $D < 20$ mm) Ellipse/Lobes a axis ($\sigma_D = 0.1$; $a/b = 0.9$; $D < 50$ mm; σ_D pertains to lobe size versus D) Ellipse/Lobes ($\sigma_D = 0.2$; $a/b = 0.6$–0.8; $D > 50$ mm)	See text; Balakrishnan and Zrnić (1990a) and Balakrishnan and Zrnić (1990b)
Orientation	Horizontally or vertically oriented; possibly tumbling	See text
Rate	$R = 88 \exp(3.45 \times 10^{-3} \lambda)$ (mm h^{-1})	Torlaschi et al. (1984)
Content	$M = R\rho(\rho_{air} V\, 3.6 \times 10^6)^{-1}$ (kg m^{-3})	Conway and Zrnić (1993)
Dielectric constant	$(\epsilon - 1)(\epsilon + 2)^{-1}$ $\approx (\rho\rho_i^{-1})(\epsilon_i - 1)/(\epsilon_i + 2)^{-1}$ $\epsilon = 3.1699 - 0.003975j$: dry ice with $\rho = 900$ (kg m^{-3}) at 0°C $\epsilon = 22.6 - 11.41j$: spongy ice (60% ice and 40% liquid by volume) $\epsilon = 80.9 - 23.865j$: wet surface at 0°C	Aydin and Zhao (1990), Longtin et al. (1987), Vivekanadan (1993a), and Doviak and Zrnić (1993)

* Z_h (mm^6 m^{-3}); q is mixing ratio (kg kg^{-1}); ρ is hydrometeor density (kg m^{-3}); Γ is the complete gamma function. Relations are for spheres unless indicated.

hail can vary from solid to spongy to porous, and the outer shell can be dry or wet. Hail density typically varies from about 400 to 900 kg m^{-3} for particles smaller than 10 mm and from 700 to 900 kg m^{-3} for particles that are larger. Hail distributions can be represented with some form of exponential or gamma function (Ulbrich and Atlas 1982) and total hail number concentrations range from 10^{-2} to 1 m^{-3} for diameters of 5–25 mm and from 10^{-6} to 10^{-2} m^{-3} for diameters larger than 25 mm (Pruppacher and Klett 1981). A summary of the characteristics of hail is presented in Table 1. When classifying hail types, dry or wet surfaces can be considered, as can size such as small (<20 mm), large (20–40 mm), and giant (>40 mm). The large and giant hail size categories in Table 2 are close to the categorizations used by the National Weather Service (severe when greater than 19 mm and significantly severe when greater than 51 mm). [Our categories differ from those (8.5, 19, and 32 mm) proposed by Lipshutz et al. (1986).]

1) REFLECTIVITY FACTOR

Mason (1971) found that Z_h in excess of 55 dBZ is appropriate to indicate hail. Vertical profiles of Z_h, the maximum Z_h, and the height of the $Z_h = 45$ dBZ level above the melting level (e.g., 1.5 km) also can be used together to indicate hail (Waldvogel et al. 1979). Our lower thresholds for hail are 45 dBZ (Table 2), although smaller Z_h have been found in hail (Walsh 1993), and values larger than 60 dBZ indicate the largest sizes of wet hail. Values of Z_h greater than 80 dBZ generally are considered extreme. The low threshold for dry hail is 5 dB lower than that for wet hail. Wetting will enhance most PR signatures of ice because of dielectric effects either on the surface of hailstones or because particle density is increased when liquid penetrates the hail's ice lattice. Also, values of Z_h greater than 80 dBZ should be considered to be exceptionally rare, even at 10-cm wavelength. The values for small and large wet hail are

TABLE 2. Thresholds for some variables to classify hail.

Hail	Z_h (dBZ)	Z_{dr} (dB)	$\lvert\rho_{hv}(0)\rvert$ (%)	K_{dp} (° km^{-1})	LDR_{vh} (dB)	δ (°)	F_{ik} (%)	F_{iz} (%)	H_{dr}	K_{dr}	T (K)
Hail ($D > 5$ mm)	45–80	−2 to 0.5	<0.97	−0.5 to 1	>−26	≠0	>0.75	>0.75	>0	>1	
Dry hail ($D > 5$ mm)	45–60	−1 to 0.5	>0.95	0 to 0.5	−26 to −18	$\lvert\delta\rvert > 1$	>0.75	>0.75	0–33	>1	<273.15
Wet hail ($D > 5$ mm)	50–80	−2 to 0.5	<0.95	−0.5 to 1	>−24	$\lvert\delta\rvert > 1$	>0.75	>0.75	>5	>2	>248.15
Small wet hail ($D < 20$ mm)	50–60	−0.5 to 0.5	0.92–0.95	−0.5 to 0.5	>−24	$\lvert\delta\rvert < 15$	>0.75	>0.75	5–33	>2	>258.15
Large wet hail ($D > 20$ mm)	55–65	−1 to 0.5	0.90–0.92	−0.5 to 1	>−20	$5 < \lvert\delta\rvert < 15$	>0.75	>0.75	18–38	>4	>248.15
Giant wet hail ($D > 40$ mm)	60–80	−2 to 0	<0.90	−0.5 to 1	>−16	$15 < \lvert\delta\rvert < 30$	>0.75	>0.75	>23	>8	>248.15

in accord with recent comparisons between observations and radar measurements (Carey and Rutledge 1998; Hubbert et al. 1998). Note that three-body scattering could produce anomalous Z_h signatures associated with hail (Zrnić 1987; Doviak and Zrnić 1993; Hubbert and Bringi 1997; Lemon 1998). If multidimensional spatial considerations of Z_h are attempted, then this anomalous signature could be used for discriminating large hail.

2) DIFFERENTIAL REFLECTIVITY

The use of Z_{dr} to identify hail size is complicated because there are no definitive relations between axis ratio and size. Small hail tends to be more spherical; therefore, $Z_{dr} \approx 0$ dB. Larger hail might be spherical, or it could be prolate to produce $Z_{dr} < 0$ dB. Tumbling motions can make nonspherical hail shapes of any size appear to be isotropic or spherical in the mean, so $Z_{dr} \approx 0$ dB.

Ground-based radar and in situ observations, as well as scattering-model studies, of hail are numerous. Ulbrich and Atlas (1984), Aydin et al. (1986b), Bringi et al. (1986), Aydin et al. (1990), Balakrishnan and Zrnić (1990b), and Zrnić et al. (1993b) provide examples from both observations and models of $-0.5 > Z_{dr} > -2$ dB for hailstones of $20 < D < 40$ mm, assuming minor axes randomly oriented in the horizontal plane (vertically oriented oblates) and larger values of Z_{dr} for smaller hailstones. Illingworth and Caylor (1986), Illingworth et al. (1987), Bringi et al. (1986b), and Husson and Pointin (1989) also found negative Z_{dr} associated with maxima of Z_h in regions of hail. Hail pad measurements by Husson and Pointin showed that hail with $D \approx 23$ mm was associated with negative Z_{dr}. Theory and observations suggest that significant negative Z_{dr} near the ground could be associated with three-body scattering (Hubbert and Bringi 1997).

Whether hail is dry or wet and spongy can also influence Z_{dr}. Longtin et al. (1987) found that wet, spongy ice spheroids exhibit increasing variation of Z_{dr} about zero with larger hail size, even for a fixed shape in the resonance scattering regime. Seliga and Bringi (1978) show that Z_{dr} for dry, oblate hailstones decreases with size and changes sign at $D \approx 50$ mm, whereas tumbling hailstones tend to produce values of $Z_{dr} \approx 0$.

Values of Z_{dr} for hail range from $-2 < Z_{dr} < 0.5$ dB in Table 2. For dry hail, $-1 < Z_{dr} < 0.5$ dB. For small wet hail, a bracket of $-0.5 < Z_{dr} < 0.5$ dB is indicated based on modeling studies and observations. The positive values account for small hailstones that might be horizontally oriented Rayleigh scatterers. Uncertainty in orientation is accounted for by straddling zero. The considerations above suggest that large and giant wet hail produce values of Z_{dr} that are possibly as large as 0.5 and 0 dB, respectively, but probably less than 0 dB (Balakrishnan and Zrnić 1990a,b; Carey and Rutledge 1998; Hubbert 1998). Because of uncertainties about the low threshold for appreciable hail sizes, we suggest

values at least as low as −2 dB (Balakrishnan and Zrnić 1990a,b). For large and giant wet hail, resonance effects could produce values of Z_{dr} that are outside of the proposed ranges. Enhanced confidence is suggested for identification of hail, dry or wet hail, and, possibly, hail size using Z_h, Z_{dr} pairs (Fig. 2a; boundaries from values provided in Table 2). In practice, extrapolated curves associated with Z_h, Z_{dr} pairs should be terminated at $Z_h \approx 80$ dBZ to avoid contamination by point scatterers such as airplanes.

3) Differential reflectivity hail signal

The differential reflectivity hail signal H_{dr} (Aydin et al. 1986b, 1990) is defined as a function of pairs of Z_h and Z_{dr} such that

$$H_{dr} = Z_h - f(Z_{dr}), \tag{1a}$$

where

$$f(Z_{dr}) = 27 \quad \text{for } Z_{dr} < 0 \text{ dB},$$
$$f(Z_{dr}) = 27 + 19Z_{dr} \quad \text{for } 0 \le Z_{dr} < 1.74 \text{ dB}, \quad \text{and}$$
$$f(Z_{dr}) = 60 \quad \text{for } Z_{dr} = 1.74 \text{ dB}. \tag{1b}$$

In (Eq. 1), $H_{dr} > 0$ indicates ice and ice–liquid mixtures. There is some evidence that larger values correspond to larger hail. Above the melting level, use of H_{dr} to detect hail is limited, because other forms of ice also can be indicated. Leitao and Watson (1984) also plot a Z_h, Z_{dr} curve that agrees with (Eq. 1) to delineate regions of rain and rain and ice mixtures. Use of H_{dr} is equivalent to partition of Z_h, Z_{dr} pairs for frozen and mixed liquid–frozen precipitation (Fig. 2a). Note, though, that it has been suggested by Brandes et al. (1993) that use of H_{dr} alone might overestimate the coverage of hail.

4) Reflectivity difference

Ice and ice–liquid mixtures may be present if the observed Z_{dp} is below the line given by

$$Z_{dp} = 1.19(Z_{hr} - 13) \text{ dB}Z, \tag{2}$$

where Z_{hr} is the Z_h (dBZ) from rain (Golestani 1989). Other curves for Z_{dp}, Z_{hr} pairs have been suggested, including $Z_{dp} = 1.12(Z_{hr} - 9)$ dBZ by Conway and Zrnić (1993), and both $Z_{hr} = 0.64Z_{dp} + 14.8$ dBZ for $1 < Z_{dp} < 20$ dBZ and $Z_{hr} = 0.88Z_{dp} + 10$ dBZ for $20 < Z_{dp} < 52$ dBZ by Aydin and Giridhar (1992). Neither Z_{dp} nor a combination Z_{dp}, Z_h have been used to classify hydrometeors, although the latter has discrimination potential. The suitable and accepted feature of Z_{dp} is the means to estimate the fraction of ice in the rain–hail mixture. Currently, we recommend that the ice fraction serve as the classification variable. To obtain its correct values, a Z_{dp} rain–hail line should be fit to actual data, so uncertainty in radar calibration is neutralized. For classification of pure hail, we suggest the fraction of ice

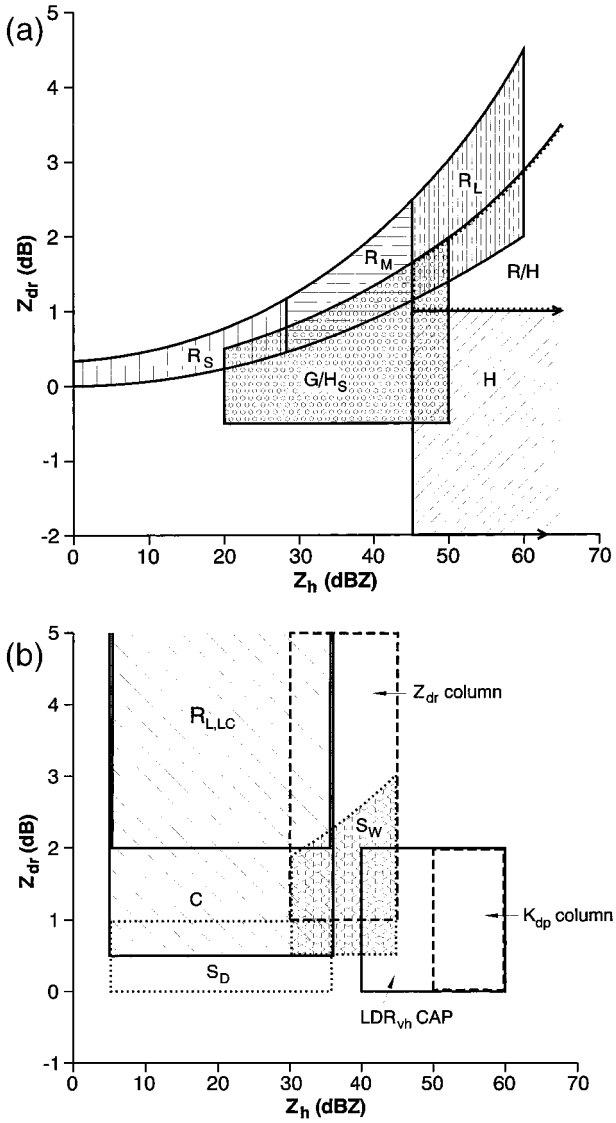

FIG. 2. (a) The two-dimensional $Z_h - Z_{dr}$ space with delineated regions of graupel–small hail (G/H_S; indicated by the area filled with hexagons); hail (H; 45°-crosshatched area); small-size rain (R_S; vertical, spaced stippling); medium-size rain (R_M; horizontal stippling), large-size rain (R_L; vertical, dense stippling), and rain–hail (R/H; area encompassed by the dotted boundary). (b) The two-dimensional $Z_h - Z_{dr}$ space with delineated regions of crystals (C; −45° crosshatched region); large raindrops in low concentrations ($R_{L,LC}$; encompassed by a solid boundary); rain-producing Z_{dr} columns (large rectangular region delineated with a dashed line); rain-producing K_{dp} columns (dashed line; small rectangle region); partially frozen–to-frozen rain-producing LDR_{vh} caps (solid line; small square region), dry snow (dotted line; horizontal rectangle), and wet snow (star-filled area). Snow refers to aggregates. Other notation is as described in (a).

F_{iz} from Z_{dp} (see section 4c) should be $F_{iz} > 0.75$ (Table 2).

5) Correlation coefficient

The thresholds in Table 2 for hail identification and size discrimination with $|\rho_{hv}(0)|$ are based on model re-

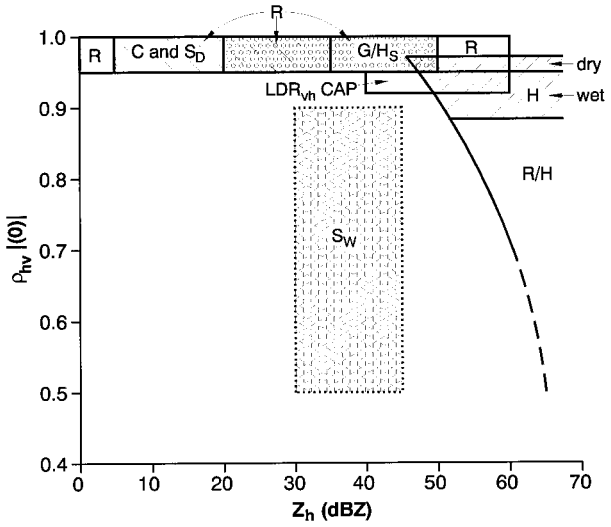

FIG. 3. The two-dimensional $Z_h - |\rho_{hv}(0)|$ space with delineated regions of crystals, graupel–small hail, dry hail, wet hail, rain, rain–hail, dry and wet snow, and partially frozen–to-frozen rain-producing LDR_{vh} caps. Other notation is as described for Fig. 2.

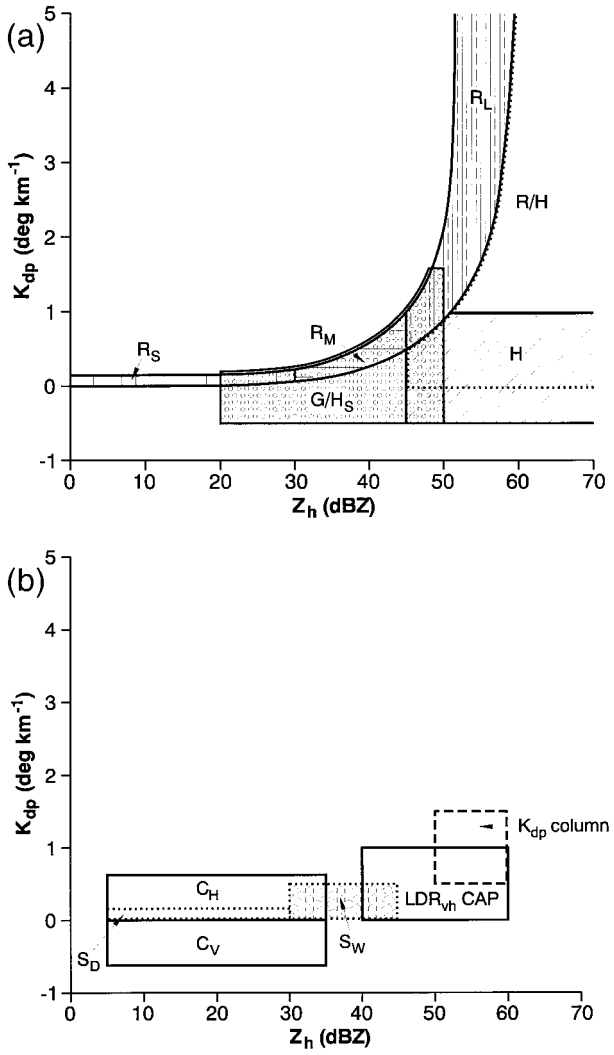

FIG. 4. (a) The two-dimensional $Z_h - K_{dp}$ space with delineated regions of graupel–small hail, hail, rain, rain–hail, small-size rain, medium-size rain, and large-size rain. Areas and boundaries are as described for (a) of Fig. 2. (b) The two-dimensional $Z_h - K_{dp}$ space with delineated regions of rain-producing K_{dp} columns, partially frozen–to-frozen rain-producing LDR_{vh} caps, horizontally and vertically oriented crystals (C_H and C_V), and dry and wet snow. Notation is as described for (b) of Fig. 2.

sults and observations by Balakrishnan and Zrnić (1990a,b), Liu et al. (1993), Bringi et al. (1996), Carey and Rutledge (1998), and Hubbert et al. (1998). Carey and Rutledge's values are larger than Hubbert et al.'s even though they both studied the same storm. Balakrishnan and Zrnić show that $|\rho_{hv}(0)|$ decreases as 1) hail size increases, 2) hail protuberance-to-diameter ratio increases, 3) hail size distributions broaden, 4) hail is wetted or becomes spongy, or 5) hail mixes with other hydrometeors with different distributions and sizes. For wet/spongy hail, there is a marked reduction in $|\rho_{hv}(0)|$ at $D \approx 20$ mm, with a more substantial reduction in $|\rho_{hv}(0)|$ at $D > 50$ mm because of resonance effects. Identification of hail is strengthened when both Z_h and $|\rho_{hv}(0)|$ in Table 2 are satisfied (Fig. 3). The hail curve at large Z_h in Fig. 3 is extrapolated from information in the cited references.

6) SPECIFIC DIFFERENTIAL PHASE

Several factors make K_{dp} insensitive to hail. First, the dielectric constant is smaller for ice than for liquid (Battan 1973). Nonetheless, on large, wet hail ($D > 20$ mm), water coatings are thin (Rasmussen et al. 1984), and there may be only marginal increases in the dielectric constant. Next, hail is found in lower concentrations than other hydrometeor types (Pruppacher and Klett 1981). Last, propagation through tumbling hail (statistically isotropic) should be insensitive to polarization. As a result, $K_{dp} \approx 0$ is common in pure hail. These factors justify the thresholds in Table 2. By extrapolating 5-cm-wavelength results from Vivekanandan et al. (1993a) to 10-cm wavelengths, we obtain for the vertically oriented hail $-1^\circ < K_{dp} < 0^\circ$ km^{-1} for $D < 20$ mm, and $0^\circ < K_{dp} < 1^\circ$ km^{-1} for larger sizes. Large scatterers can produce δ, which complicates K_{dp} estimations. Although regions of δ can be recognized in radial profiles of ϕ_{dp}, methods to separate propagation contributions to ϕ_{dp} from δ are prone to errors of about $\pm 5^\circ$ (Hubbert and Bringi 1995). Table 2 shows values of $-0.5^\circ < K_{dp} < 1^\circ$ km^{-1} for general hail identification, whereby the negative range of values is smaller than theoretical extrapolation from Vivekanandan et al. (1993a); we opt for the smaller range, because, in our data analysis, we have not encountered significant negative K_{dp} in hail. Smaller amplitude ranges about zero are associated with dry and/or smaller particles and larger ranges are associated with larger wet particles. Figure

4a shows that hail identification confidence can be increased with Z_h, K_{dp} pairs. Similarly to H_{dr}, one can define K_{dr} as the distance (along a constant Z_h line) from the rain curve in the K_{dp}, Z_h plane (Balakrishnan and Zrnić 1990a; Walsh 1993),

$$K_{dr} = 10^{[0.125(Z_h - 49)]} - K_{dp} - 20. \quad (3)$$

Values of K_{dr} should be greater than 1° km^{-1} for hail, greater than 2° km^{-1} for wet hail, and greater than 4° and 8° km^{-1} for large and giant hail, respectively. Walsh (1993) found that K_{dr} helped to indicate the presence of ice particles with $D > 6$ mm. Last, the fraction of ice F_{ik} from K_{dp} (section 4c) should be $F_{ik} > 0.75$ to classify hydrometeors in the pure hail category.

7) BACKSCATTER DIFFERENTIAL PHASE

Balakrishnan and Zrnić (1990b) modeled values of δ for dry and wet hail with axis ratios of 0.8 and for wet, spongy hail with axis ratios of 0.6 and 0.8. They noted that dry hail produces values of $\delta \approx 0$ for $D < 40$ mm; hence, we set $|\delta| = 1$ (Table 2). For wet hail with $D \approx$ 7–10 mm (oriented oblates, minor axis vertical), scattering models produce $0° > \delta > -5°$. At $D \approx 10$ mm, there is a sharp transition, with $\delta \approx 10°$. Last, when $D \approx 50$ mm, δ is substantially negative ($-30°$ to $-50°$). Spongy hail, with an axis ratio of 0.8, behaves similarly to wet hail except that the sharp transition shifts to $D \approx 15$ mm. Scattering by spongy hail with an axis ratio 0.6 produces similar results, but the magnitudes of δ are larger. An observational study by Zrnić et al. (1993b) suggests that large negative values of δ might indicate large hail in accord with the scattering-model results. They also noted that smaller negative values might indicate lower concentration of large hail and that positive values might indicate smaller hail. For large tumbling hailstones, $\delta \approx 0$, because they appear spherical in the mean. The thresholds in Table 2 are derived from the scattering models of oblate spheroids. Absolute values for δ in Table 2 accommodate both vertical and horizontal hydrometeor alignment because hail orientation generally is not known.

8) LINEAR DEPOLARIZATION RATIO

Many previous LDR_{vh} measurements associated with hail are at a 3-cm wavelength (e.g., Bringi et al. 1986b; Tuttle et al. 1989; Brandes et al. 1995). These measurements suggest values of $LDR_{vh} > -25$ dB for hail and values of -18 to -8 dB for unaligned or nonspherical hydrometeors that often are large, such as giant hail. Large values of LDR_{vh}, even at 3-cm wavelength, generally rule out smooth, smaller hail. Kennedy et al. (1997) suggest slightly smaller values of LDR_{vh} for hail discrimination at 10-cm wavelength. The observations and calculations of Frost et al. (1989, 1991) at 10-cm wavelength, however, indicate that the 3-cm wavelength values generally are applicable. In support of Frost et al.'s work, Vivekanandan et al.'s (1993b) scattering model results of LDR_{vh} include $-28 < LDR_{vh} < -15$ dB for dry hail and $-24 < LDR_{vh} < -22$ dB for wet hail, though they noted that ranges of these values are sensitive to assumptions about axis ratios, orientation, etc. Aydin and Zhao (1990) also carried out extensive modeling studies of hail and showed that hail can produce a wide range of LDR_{vh}, varying from less than -25 dB to greater than -15 dB (the larger values are caused by resonance effects). In addition, observational studies by Carey and Rutledge (1998) and Hubbert et al. (1998) at 10-cm wavelength with the CSU-CHILL radar include values of LDR_{vh} greater than -27 to -25 associated with hail and values of LDR_{vh} as large as -15 to -13 with wet, large/giant size hail. Based on the studies above, we suggest a threshold of LDR_{vh} greater than -26 dB to indicate hail in general, -26 to -18 dB for dry hail, greater than -24 dB for wet and small wet hail, greater than -20 dB for large wet and spongy hail, and greater than -16 dB for giant hail or large, water-coated hail. Confidence in discrimination of hail should be enhanced if the thresholds for Z_{dr} and LDR_{vh} (Table 2) are both valid (Fig. 5). Holler et al. (1994) also employed Z_{dr}, LDR_{vh} pairs at a 5-cm wavelength for hail discrimination; our values are similar to theirs. Last, Illingworth et al. (1986) found that a local increase of 6 dB in LDR_{vh} might be indicative of a hail shaft. This information also could help to discriminate hail.

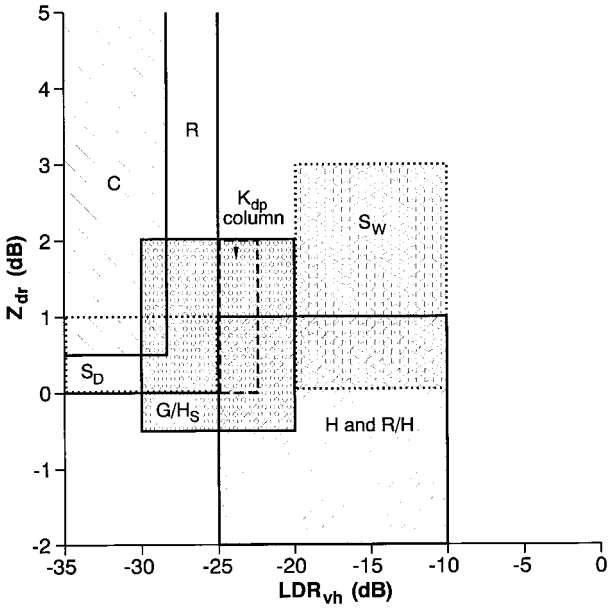

FIG. 5. The two-dimensional $Z_{dr} - LDR_{vh}$ space with delineated regions of crystals, graupel–small hail, hail, rain, rain–hail, dry and wet snow, and rain-producing K_{dp} columns. Other notation is as described for Fig. 2.

b. Graupel and/or small hail

Graupel ($0.5 < D < 5$ mm) and small hail ($5 < D < 20$ mm) often coexist and are indistinguishable. Even

if graupel–small hail are physically distinguishable from each other, and one of the species is dominant, it may not be possible to determine which one it is. Thus, we are compelled to consider the two together. The density of graupel–small hail can range from 100 to 900 kg m^{-3}, size distributions can be represented by exponential or gamma functions, and number concentrations are on the order of $1–10^3$ m^{-3} (Pruppacher and Klett 1981). The shapes of graupel–small hail can be spherical or can be conical with axis ratios both larger and smaller than unity (Bringi et al. 1984; Aydin and Seliga 1984). In the study by Bringi et al. (1984), graupel with $2a$ less than 1 mm are assumed to be spherical, graupel with $1 \leq 2a \leq 4$ mm are conical with $a/b = 0.5$, and graupel with $4 < 2a < 9$ mm are conical with $a/b = 0.75$. Both smaller and larger particles might be spherical or irregular (e.g., lump graupel; highly irregular shaped rimed crystals and aggregates) in shape based on in situ observations. Low-density graupel sometimes is conical in shape, which might reveal its presence through distinct scattering properties related to aspect ratios (Aydin and Seliga 1984). In general, graupel–small hail tend to be relatively smooth in comparison with some large hailstones. The fall orientation of graupel–small hail is not known with great certainty, but some investigators hypothesize that the larger of these hydrometeors probably tumble, though conical graupel may have a preferential fall orientation (List and Schemenaur 1971; Pruppacher and Klett 1981). Some graupel may fall with their largest axis in the horizontal, whereas others may fall with their largest axis in the vertical. A summary of these details is presented in Table 3.

1) Reflectivity factor

During the Cooperative Convective Precipitation Experiment (CCOPE) in Montana (Bringi et al. 1984) and the May Polarization Experiments (MAYPOLE) in Colorado (Bringi et al. 1986a), graupel measurements by radar were compared with observations made with aircraft. In both experiments, graupel–small hail as large as $D \approx 9$ mm were found in regions where measured Z_h was below 35 dBZ. In addition, Z_h computed from information obtained by precipitation probes ranged between 20 and 35 dBZ in the CCOPE storms. Similar Z_h values were measured in the MAYPOLE storms, but they were about 5 dBZ higher than was predicted by a scattering model. Bringi et al. attribute these higher values to the presence of wet graupel. They also might be associated with higher densities associated with these graupel particles. Walsh (1993) and Aydin et al. (1993) report similar results from an Oklahoma storm. Based on these findings, we associate dry, low-density graupel–small hail with $Z_h < 35$ dBZ (Table 4). In addition, wet, high-density graupel–small hail is associated with Z_h of 30–50 dBZ [e.g., Aydin and Seliga (1984) suggest $Z_h < 45$ dBZ for graupel]. Note that, according to Vivekanandan et al. (1990), Z_h probably is insensitive to whether graupel–small hail is spherical or conical.

2) Differential reflectivity

Graupel–small hail can be identified by negative Z_{dr} if they are elongated and fall in a vertically oriented manner (Aydin and Seliga 1984; Aydin et al. 1984). Thus, we set a lower threshold of -0.5 dB in Table 4. On the other hand, positive values of Z_{dr} could be produced by graupel–small hail if they are more oblate in shape and fall in a horizontally oriented manner (Bringi et al. 1984, 1986a). Aydin and Seliga (1984) show, using scattering-model results, that canting of 0°–30° reduces Z_{dr} by 0–1 dB for wet, high-density graupel and by 0–0.5 dB for dry, low-density graupel. Also, wetting of ice particles tends to enhance PR signatures because of dielectric constant effects and possible increases in particle density; thus, the upper threshold is 2 dB for wet, high-density graupel versus 1 dB for dry, low-density graupel. These results agree with the observations and computed values presented by Bringi et al. (1984, 1986a), who used particle probe data and assumed random canting to obtain $Z_{dr} < 2.5$ dB for graupel. It is noted, though, that Aydin and Zhao (1990) modeled values of Z_{dr} up to 3 dB for some shapes of graupel. Figure 2a shows the space where Z_h, Z_{dr} pairs should be used to enhance confidence in classification of graupel–small hail.

3) Reflectivity difference and hail signal

The fraction of ice from Z_{dp} should be $F_{iz} > 0.75$ for pure graupel–small hail. Differential reflectivity hail signal in Table 4 should be used as described for hail. Values of $H_{dr} > 0$ are suggested for dry graupel–small hail and of $H_{dr} > 5$ for wet, high-density particles.

4) Correlation coefficient

Because graupel–small hail are relatively smooth, we suggest a low threshold of $|\rho_{hv}(0)| > 0.95$ (Table 4). This value is derived from measurements and scattering-model studies of small hail (Balakrishnan and Zrnić 1990b). Melting graupel/small hail mixed with rain could have a lower $|\rho_{hv}(0)|$ [0.92 in the model of Aydin and Zhao (1990)], but we classify such a combination of hydrometeors as rain–wet hail mixture (Table 7, presented later). Identification of graupel–small hail should be strengthened when the threshold ranges for both Z_h and $|\rho_{hv}(0)|$ are satisfied (Fig. 3).

5) Specific differential phase

Not much is known about K_{dp} in graupel, though signals in small hail should be similar to those discussed for hail. A lower threshold in Table 4 of $-0.5°$ km^{-1} should accommodate vertically oriented wet graupel,

TABLE 3. Equations and parameters for graupel–small hail.

Parameter	Equations	Reference
Distribution	$n(D) = n_o \exp(-D\lambda)$ (m^{-4}) exponential distribution $n(D) = n_o D^{\mu} \exp(-D\lambda)$ (m^{-4}) gamma distribution See hail (Table 1) for high-density particles	Lin et al. (1983), Ferrier (1994), and Ulbrich and Atlas (1982)
Total number	$N_t = n_o \lambda^{-1}$ (m^{-3}) exponential distribution $N_t = n_o \lambda^{-(1+\mu)} \Gamma(1 + \mu)$ (m^{-3}) gamma distribution	Lin et al. (1983) and Ferrier (1994)
Slope	$\lambda = [(\rho n_o \pi)/(\rho_{air} q)]^{-1/4}$ (m^{-1}) (low density) exponential distribution $\lambda = \{[(\Gamma(4 + \mu)\rho N_t \pi]/[6\Gamma(1 + \mu)\rho_{air} q]\}^{-1/3}$ (m^{-1}) (low density) gamma distribution See hail (Table 1) for high-density particles	Lin et al. (1983) and Ferrier (1994)
Intercept	$n_o = 8 \times 10^6$ (m^{-1}) (low density) (range of 4×10^4–1×10^7) exponential distribution $n_o = N_t \lambda^{-(1+\mu)}[\Gamma(1 + \mu)]^{-1}$ ($m^{-(4+\mu)}$) gamma distribution See hail (Table 1) for high-density particles	Hauser and Ameyanc (1986), Lin et al. (1983), and Ferrier (1994)
Median diam (D_o) and mass-weighted mean diam (D_m)	$D_o = 3.67\lambda^{-1}$ (m); $D_m = 4\lambda^{-1}$ (m) exponential distribution $D_o = (3.67 + \mu)\lambda^{-1}$ (m); $D_m = [\Gamma(5 + \mu)/\Gamma(4 + \mu)]\lambda^{-1}$ (m) gamma distribution	Doviak and Zrnić (1993)
Density	$\rho_{low\,density} = 150.0$ (kg m^{-3}) (could range from 150 to 900 kg m^{-3}) $\rho_{high\,density} = 900.0$ (kg m^{-3}) Note that density can vary considerably within a storm and from storm to storm	Locatelli and Hobbs (1974) and Pruppacher and Klett (1981)
Fall velocity*	$V_{low\,density} = 1.23 Z_h^{0.103}$ (m s^{-1}) $V = [(4\rho D g)/(3\rho_{air} C_d)]^{0.5}$ (where $0.45 < C_d < 2.0$) See hail (Table 1) for high-density particles	Locatelli and Hobbs (1974), Pruppacher and Klett (1981), and Conway and Zrnić (1993)
Shape	Spherical to conical	Pruppacher and Klett (1981)
Orientation	Stable horizontal or vertical orientation for low Reynolds numbers (apex down and up are possible stable orientations); oscillations for Reynolds numbers of >200 to 800; tumbling for Reynolds numbers of >300 to 1000	Pruppacher and Klett (1981) and List and Schemenauer (1971)
Rate	$R_{low\,density} = 3.6 \times 10^6 M\rho V$ (mm h^{-1}) See hail (Table 1) for high-density particles	Herzegh and Hobbs (1980), Conway and Zrnić (1993), and Cheng and English (1983)
Content*	$M_{low\,density} = 1.26 \times 10^{-6} Z_h^{0.571}$ (kg m^{-3}) See hail (Table 1) for high-density particles	Hauser and Ameyanc (1986) and Conway and Zrnić (1993)
Dielectric constant	$(\epsilon - 1)(\epsilon + 2)^{-1}$ $\approx (\rho\rho_i^{-1})(\epsilon_i - 1)/(\epsilon_i + 2)^{-1}$ $\epsilon = 1.97 - 0.271j$: dry ice with $\rho = 500$ (kg m^{-3}) at 0°C $\epsilon = 22.6 - 11.41j$: spongy ice (60% ice and 40% liquid by volume) $\epsilon = 66.47 - 37.02j$: wet surface	Longtin et al. (1987) and Vivekanadan (1993a)

* Z_h (mm^6 m^{-3}); q is mixing ratio (kg kg^{-1}); ρ is hydrometeor density (kg m^{-3}); Γ is the complete gamma function; wet, high-density graupel and small hail variables are computed similarly to hail in Table 1; for spheres unless indicated.

TABLE 4. Thresholds for some variables to classify graupel–small hail.

Graupel–small hail	Z_h (dBZ)	Z_{dr} (dB)	$\lvert\rho_{hv}(0)\rvert$ (%)	K_{dp} (°km^{-1})	LDR_{vh} (dB)	δ (°)	F_{ik} (%)	F_{iz} (%)	H_{dr}	K_{dr}	T (K)
Graupel–small hail	20–50	−0.5 to 2	>0.95	0–1.5	<−20	$\lvert\delta\rvert < 1$	>0.75	>0.75	>0	>1	
Dry low density	20–35	−0.5 to 1	>0.95	0–0.5	<−25	$\lvert\delta\rvert < 1$	>0.75	>0.75	>0	>1	<273.15
Wet high density	30–50	−0.5 to 2	>0.95	0–1.5	−20 to −30	$\lvert\delta\rvert < 1$	>0.75	>0.75	>5	>2	>258.15

and the upper threshold of 1.5° km^{-1} should be adequate for horizontally oriented small hail (oblate and wet). As described in section 3c on rain, however, if Z_h is greater than $Z_h(K_{dp})$, it is possible that an ice or an ice–rain mixture exists. The indication for graupel–small hail should be strengthened if both $-0.5° < K_{dp} < 1.5°$ km^{-1} and $20 < Z_h < 50$ dBZ (Fig. 4a) are satisfied. The fraction of ice from K_{dp} should be F_{ik} greater than 0.75 for pure graupel–small hail. Also, values of K_{dr}, which helps to discriminate between rain and ice or rain–ice mixtures, should be greater than 1° km^{-1} for graupel–small hail in general, and greater than 2° km^{-1} for wet, high-density particles.

6) Backscatter differential phase

Graupel particles are small in comparison with a 10-cm wavelength and generally are smooth. Thus, $|\delta|$ less than 1° can be associated with graupel.

7) Linear depolarization ratio

Bringi et al.'s (1986a) 3-cm wavelength scattering-model values of LDR_{vh} include $-25 < \mathrm{LDR}_{vh} < -20$ dB for conical graupel and between $-26 < \mathrm{LDR}_{vh} < -24$ dB for melting graupel. In addition, Vivekanandan et al. (1990) show that larger LDR_{vh} is possible for conical graupel than for spheroidal graupel. The LDR_{vh} enhancement probably is due to irregularly shaped or tumbling particles. Wetting of ice surfaces also increases LDR_{vh}. Computations of LDR_{vh} in dry graupel at a 10-cm wavelength (Frost et al. 1989, 1991) are $-26 < \mathrm{LDR}_{vh} < -22$ dB and agree with the Rayleigh–Gans scattering model of randomly oriented oblate spheroids. Slightly higher LDR_{vh} values for graupel–small hail are expected for the 3-cm wavelength because of resonance effects. The thresholds in Table 4 are derived from the model and observation studies by Bringi et al. (1986a) and Vivekanandan et al. (1990) and are in accord with measurements and computations of Frost et al. (1989, 1991). Figure 5 shows the parameter space where Z_{dr}, LDR_{vh} pairs should strengthen PR classification confidence of graupel/small hail. This space is similar to that proposed by Holler et al. (1994) for PR variables at a 5-cm wavelength.

c. Rain

Precipitating liquid particles include drizzle and raindrops. Our discussion focuses on rain, and drizzle can be considered to be very small raindrops for practical purposes in this paper. A characteristic that sets rain apart from other precipitating particles is the dependence of drop axis ratio on size. Axis ratios commonly are related to drop sizes through equivalent diameter D_e (Pruppacher and Klett 1981); several relations exist, including

$$a/b = 1.03 - 0.062D_e, \quad (4)$$

where D_e is in millimeters, a is the horizontal axis, and b is the vertical axis (Pruppacher and Beard 1970; Pruppacher and Pitter 1971). Studies by Jones (1959), Jameson and Beard (1982), and Goddard et al. (1982) show, with concern, that in heavier rain events a large range in axis ratios might be expected with even prolates possible (though the latter are likely transient oscillations). After nearly two decades, raindrop axis ratio and its functional form, as well as the importance of drop oscillations, are under renewed scrutiny (e.g., Beard and Feng 1991; Beard et al. 1991; Tokay and Beard 1996; Bringi et al. 1998). Nevertheless, Eq. (4) and others' similar relations specify that, for D greater than 1 mm, drops become increasingly oblate with size. Raindrops generally fall with their minor axis oriented in the vertical, though a rare few drops might be temporarily elongated in the vertical (Takahashi and Kuhara 1993), possibly because of oscillations, collisions, or both. A theoretical study by Beard and Jameson (1983) and radar observations by Hendry et al. (1987) suggest that mean raindrop canting typically is less than 5°–10°. Size distributions can be approximated by exponential (Marshall and Palmer 1948) or gamma functions (Ulbrich 1983) for mean droplet spectra, but extreme local variations from these are observed (e.g., Rauber et al. 1991; Young 1993; Joss and Zawadski 1997). For the largest rain drops, $D \approx$ 3–5 mm; however, values as large as $D \approx$ 6–8 mm are documented (e.g., Rauber et al. 1991). Total number concentrations of rain are on the order of 10^3 to 10^4 m^{-3}, but very large drops are usually present in low concentrations ($<10^4$ m^{-3}). Details about the physical attributes of raindrops are presented in Table 5.

The National Weather Service classifies rain in six categories that are related to the reflectivity factor (Lipschutz et al. 1986; Bluestein 1992) including light ($Z_h < 30$ dBZ), moderate ($30 < Z_h < 40$ dBZ), heavy ($40 < Z_h < 45$ dBZ), very heavy ($45 < Z_h < 50$ dBZ), intense ($50 < Z_h < 57$ dBZ), and extreme ($Z_h > 57$ dBZ). For applications in numerical modeling, sizes of drops are important because they influence residence time in a storm and microphysical interactions. Polarimetric radar data are suitable for determining distribution and median sizes of raindrops. (Pertinent equations are presented in section 4.) Even if the median sizes cannot be determined (e.g., if Z_{dr} is not available, or hail is contaminating PR signals), it still may be possible to categorize rain into a few classes according to the median diameter D_o. We prescribe three categories in Table 6: small ($D_o < 1$ mm), medium ($1 < D_o < 2$ mm), and large ($D_o > 2$ mm).

1) Reflectivity factor

The Z_h thresholds in Table 6 are chosen to be compatible with Z_{dr} by substituting [Eq. 6, section 3c2] into Eq. (5), where Z_{hr} is found by equating the Marshall–Palmer relation ($Z_h = 200R^{1.6}$) to a relation $R(Z_h, Z_v)$,

where R is precipitation rate, proposed by Sachidananda and Zrnić (1987):

$$Z_{\rm hr} = 86.7(Z_h/Z_v)^{12.96}, \quad (5)$$

where the units of Z are mm^6 m^{-3}. Maximum values of Z_h in pure rain are $\approx$ 60 dBZ.

2) Differential reflectivity

For individual raindrops, the axis ratio and, thus, $Z_{\rm dr}$ are uniquely related to size, but, for a distribution, that relation depends on the parameters of the distribution (e.g., Seliga and Bringi 1976; Hall et al. 1980; Bringi et al. 1991) and drop behavior (highlighted below). [Jameson (1985) and Zrnić and Doviak (1989) found that small canting of raindrops has a negligible influence on $Z_{\rm dr}$ observations.] A relation between D_o and $Z_{\rm dr}$ for rain is generated with a least squares fit of a second-order polynomial to a set of D_o, $Z_{\rm dr}$ pairs, assuming a gamma drop size distribution and Eq. (4). The parameters of the distribution are varied to obtain

$$D_o = 0.495 + 0.739Z_{\rm dr} + 0.015Z_{\rm dr}^2, \quad (6)$$

where D_o is in millimeters and $Z_{\rm dr}$ is in decibels. This equation is similar to the one proposed by Illingworth and Caylor (1989) and produces results comparable to those described by Al-Khatib et. al. (1979). The behavior of Eq. (6) is such that a larger D_o produces a larger $Z_{\rm dr}$. The $Z_{\rm dr}$ thresholds in Table 6 recommended to discriminate rain satisfy Eqs. (4), (5), and (6).

As expected, there is a general trend for larger values of $Z_{\rm dr}$ to be found with larger values of Z_h. This is not always the case, however. For example, Illingworth et al. (1987) and Bringi et al. (1991, 1993, 1997, 1998) found that very large $Z_{\rm dr}$ (1.5–5.5 dB) with small Z_h (5–40 dBZ) probably indicate low concentrations of very large drops with $D \approx$ 6–8 mm. Aircraft observations described by Bringi et al. (1991, 1997, 1998) and others strongly support this theory. Rauber et al. (1991) also have observed very large raindrops in low concentrations in shallow Hawaiian precipitation systems. Based on these observations, we make an accommodation in Table 6 for small concentrations of large raindrops (and paucity of small drops).

Often, a column of large values of $Z_{\rm dr}$ extends from below the melting level to temperatures as low as -10°C or so. These ''$Z_{\rm dr}$ columns'' are associated with larger raindrops in many deep convective storms, where the drops probably are growing by coalescence. (We should note there could be other explanations for such columns that are beyond the scope of this paper.) A large source of hail embryos may be provided via freezing of drops in these columns (Conway and Zrnić 1993, Askelson et al. 1997, 1998; Carey and Rutledge 1998; Hubbert et al. 1998). Typically, the $Z_{\rm dr}$ column is a region with values of $30 < Z_h < 45$ dBZ, $1 < Z_{\rm dr} < 3$ dB, $K_{\rm dp} \approx 0°$ km^{-1}, reduced values of $|\rho_{hv}(0)|$, and larger values of LDR$_{vh}$ than usually are found with rain (Conway and Zrnić 1993; Hubbert et al. 1998). Values of the PR variables in the $Z_{\rm dr}$ column also are included in Table 6.

The Z_h, $Z_{\rm dr}$ pairs in Fig. 2a that define values associated with rain are a composite of observations (e.g., Aydin et al. 1986a,b; Leitao and Watson 1984; Illingworth 1988; Balakrishnan and Zrnić 1990a) and some of our recent simulations. We also have added subdelineations to the rain region to show small, medium, and large median drop sizes. In addition, we have included a parameter space for Z_h, $Z_{\rm dr}$ pairs to indicate increased classification confidence of large drops in low number concentrations in Fig. 2b. Last, the parameter space for Z_h, $Z_{\rm dr}$ pairs that define the $Z_{\rm dr}$ column is in Fig. 2b. Most of these Z_h, $Z_{\rm dr}$ regions are defined from the Z_h and $Z_{\rm dr}$ thresholds in Table 6. The largest values of $Z_{\rm dr}$ in Figs. 2a,b is 5 dB, which approximately corresponds to the largest $Z_{\rm dr}$ measured with PR and the largest drop sizes observed in situ with aircraft (though larger values for both certainly are possible).

3) Reflectivity difference and hail signal

As noted by Golestani (1989), pure liquid-phase hydrometeors may be present if values of $Z_{\rm dp}$ fall along the line given by Eq. (2). In addition, the fraction of ice from $Z_{\rm dp}$ should be $F_{\rm iz} < 0.25$ for pure rain (Table 6). Values of $H_{\rm dr}$ less than 0 can signify rain (Table 6). Above the freezing level, $H_{\rm dr} < 0$ can indicate other hydrometeor types as well; therefore, $H_{\rm dr}$ should be used only at $T > 0$°C for rain.

4) Correlation coefficient

In theory, values of $|\rho_{hv}(0)|$ in rain are generally close to unity. Slight departures from near unity are due to a continual change in shape (a ''breadth of the axis ratios'') through typical rain size distributions. Jameson and Dave (1988) imply that drop oscillations also can reduce $|\rho_{hv}(0)|$ from unity because the ΔZ_h and ΔZ_v are not identical for the same increment in the drop size. Moreover, some reduction in correlation can be expected from effects such as drop oscillations, coalescence, and breakup, all of which can occur on the scale of the radar dwell time (Doviak and Zrnić 1993). For pure rain, the theoretical value for $|\rho_{hv}(0)|$ is 0.98, which is consistent with observations that values of $|\rho_{hv}(0)|$ are greater than 0.97 (Balakrishnan and Zrnić 1990b), 0.99 (Illingworth and Caylor 1991), and 0.975 in small drops (Liu et al. 1993). A threshold of 0.97 is assigned for smaller drops, and a value of 0.95 for larger sizes accommodates the effects of oscillations and canting. Pairs of Z_h, $|\rho_{hv}(0)|$ in Fig. 3 indicate enhanced confidence in rain discrimination over what would be observed by either variable. There is recent observational and theoretical evidence of decreased $|\rho_{hv}(0)|$ near the top of $Z_{\rm dr}$ columns and in association with frozen and/or freezing drops in the ''LDR$_{vh}$ cap'' (Hubbert et al. 1995, 1998 Jameson et al. 1996). In these regions, $|\rho_{hv}(0)|$ may be as low as 0.96

TABLE 5. Equations and parameters for rain (and rain when mixed with wet hail).

Parameter	Equations	Reference
Distribution	$n(D) = n_o \exp(-D\lambda)$ (m^{-4}) exponential distribution $n(D) = n_o D^{\mu} \exp(-D\lambda)$ (m^{-4}) gamma distribution $n(D) = n_o D^{2.5} \exp(-D\lambda)$ (cm^{-4}) gamma distribution	Lin et al. (1983), Ulbrich (1983), Willis (1984), and Ferrier (1994)
Number	$N_t = n_o \lambda^{-1}$ (m^{-3}) exponential distribution $N_t = n_o \lambda^{-(1+\mu)} \Gamma(1 + \mu)$ (m^{-3}) gamma distribution	Lin et al. (1983), Ulbrich (1983), and Ferrier (1994)
Slope	$\lambda = [(\rho n_o \pi)/(\rho_{air} q)]^{-1/4}$ (m^{-1}) exponential distribution $\lambda = \{[(\Gamma(4 + \mu)\rho N_t \pi]/[6\Gamma(1 + \mu)\rho_{air} q]\}^{-1/3}$ (m^{-1}) gamma distribution $\lambda = 3.483(\rho_{air} q)^{-0.168}$ (cm^{-1}; cgs units); gamma distribution ($\mu = 2.5$)	Lin et al. (1983), Ulbrich (1983), and Ferrier (1994)
Intercept	Exponential distribution (m^{-4}): $n_o = 8 \times 10^6$ (general) $n_o = 2.2 \times 10^7$ (hurricane) $n_o = 2.7 \times 10^7$ (convective storms)	Lin et al. (1983) and Lord et al. (1984)
	Gamma distribution [$m^{-(4+\mu)}$ except where noted] $n_o = n_t \lambda^{-(1+\mu)}[\Gamma(1 + \mu)]^{-1}$ $n_o = 30.07(\rho_{air} q)^{-0.092}$ [$cm^{-(4+\mu)}$ cgs units; $\mu = 2.5$] $n_o = 1.48 \times 10^7$; 1.13×10^8; 9.58×10^8 ($\mu = 0.27$; -1.03; -1.39) (orographic) $n_o = 1.13 \times 10^5$; 1.18×10^6; 2.35×10^6; 1.12×10^6 ($\mu = 1.63$; 1.01; 1.01; 0.40) (thunderstorm) $n_o = 3.21 \times 10^3$; 7.19×10^5; 8.56×10^6; 2.75×10^7 ($\mu = 4.65$; 1.01; 0.18; -0.79) (stratiform) $n_o = 7.65 \times 10^2$; 4.14×10^5; 1.04×10^7; 6.27×10^5; 3.47×10^5; 8.92×10^6 ($\mu = 5.04$; 1.63; 0.01; -1.34; -1.79; -3.42) (shower)	Ferrier (1994); Ulbrich (1983)
Median diam (D_o) and mass-weighted mean diam (D_m)	Exponential distribution: $D_o = 3.67\lambda^{-1}$ (m); $D_m = 4\lambda^{-1}$ (m)	Doviak and Zrnić (1993); See text
	Gamma distribution: $D_o = (3.67 + \mu)\lambda^{-1}$ (m); $D_m = [\Gamma(5 + \mu)/\Gamma(4 + \mu)]\lambda^{-1}$ (m)	
	Gamma distribution (from Z_{dr}): $D_o = 1000(0.495 + 0.739Z_{dr} + 0.015Z_{dr}^2)$ (m)	Ulbrich (1983) Ulbrich and Atlas (1998)
	Gamma distribution [From R (mm h^{-1}); same as intercept section]: $D_o = \epsilon R^{\delta}$, where $\delta = (4.67 + \mu)^{-1}$ and $\epsilon = (3.67 + \mu)[33.31 n_o \Gamma(4.67 + \mu)]^{-\delta}$ (Typically, low ϵ and high δ is from small D_o, and high ϵ and low δ is from large D_o) $\epsilon = 0.080$; 0.055; 0.031; ($\delta = 0.23$; 0.28; 0.31) (orographic) $\epsilon = 0.130$; 0.101; 0.090; 0.118; ($\delta = 0.16$; 0.18; 0.18; 0.20) (thunderstorm) $\epsilon = 0.114$; 0.110; 0.082; 0.077; ($\delta = 0.11$; 0.18; 0.21; 0.26) (stratiform) $\epsilon = 0.129$; 0.106; 0.081; 0.069; 0.095; 0.013; ($\delta = 0.10$; 0.16; 0.22; 0.30; 0.35; 0.80) (shower)	
Density	$\rho = 1000$ (kg m^{-3})	Pruppacher and Klett (1981)
Fall velocity	$V = 3.28Z_h^{0.088}$ (m s^{-1}) $V = 842D^{0.8}$ (m s^{-1})	Hauser and Ameyanc (1986), Lin et al. (1983), and Gunn and Kinzer (1949)
Shape	Oblate spheroid [$a/b = 1.03 - 0.062d_e$ (mm) where d_e is equivalent spherical diameter]	Pruppacher and Pitter (1971)
Orientation	Horizontally oriented; little canting; possible oscillations	Pruppacher and Klett (1981), Beard and Jameson (1983), and Tokay and Beard (1995, 1996)
Rate*	$R = 3.65 \times 10^{-2} Z_h^{0.625}$; $R < 20$ mm h^{-1} $R = 1.70 \times 10^{-2} Z_h^{0.714}$ (mm h^{-1}) (Z_h truncated at 51 dBZ for arid/semiarid) $R = 1.00 \times 10^{-2} Z_h^{0.833}$ (mm h^{-1}) (Z_h truncated at 55 dBZ for maritime/tropical/other) $R = 6.84 \times 10^{-3} Z_h^{-3.86} Z_v^{4.86}$; $20 < R < 50$ mm h^{-1} $R = 1.00 \times 10^{-3} Z_h^{0.920} 10^{-0.369 Z_{dr}}$; $20 < R < 50$ mm h^{-1} $R = 40.6K_{dp}^{0.866}$ (mm h^{-1}); $R > 50$ mm h^{-1} (Ryzhkov recently suggested $R > 5$ mm h^{-1}) $R = 52.0K_{dp}^{0.960} Z_{dr}^{-0.447}$ (mm h^{-1}); $R > 20$ mm h^{-1}	Kessler (1969), Vieux and Bedient (1998), Aydin et al. (1995), Sachidananda and Zrnić (1987), Gorgucci et al. (1995), Ryzhkov and Zrnić (1995a) and similar ones by Jameson (1991)

TABLE 5. Continued.

Parameter	Equations	Reference
Content*	$M = R\rho(\rho_{air}V\ 3.6 \times 10^6)^{-1}$ (kg m^{-3}) in general $M = 3.44 \times 10^{-6}\ Z_h^{0.571}$ (kg m^{-3}) $M = 1.06 \times 10^{-6}\ Z_h^{-3.32} Z_v^{4.18}$ (kg m^{-3}) $M = 1.63 K_{dp}^{0.760}$ (kg m^{-3}) $M = 3.11 K_{dp}^{0.918} Z_{dr}^{-0.764}$ (kg m^{-3})	Doviak and Zrnić (1993) and Ryzhkov and Zrnić (1995a)
Dielectric constant	$(\epsilon - 1)(\epsilon + 2)^{-1}$ $\approx (\epsilon_i - 1)/(\epsilon_i + 2)^{-1}$ $\epsilon = 80.6 - 23.8645j$: liquid with $\rho = 1000$ (kg m^{-3}) at 0°C $\epsilon = 70.9 - 29.4j$: liquid with $\rho = 1000$ (kg m^{-3}) at 10°C	Aydin and Zhao (1990) and Vivekanadan (1993a)

* Z_h (mm^6 m^{-3}); Z_{dr} (dB); K_{dp} (° km^{-1}); q is mixing ratio (kg kg^{-1}); ρ is hydrometeor density (kg m^{-3}); D_e is equivalent diameter; Γ is the complete gamma function; for spheres unless indicated.

and 0.92, respectively. It should be remembered that these observations are not of pure rain in a strict sense.

5) SPECIFIC DIFFERENTIAL PHASE

Signatures in K_{dp} are produced by statistically anisotropic hydrometeors such as rain when drops are larger than about 1 mm. Therefore, K_{dp} can be used to isolate the presence of rain from statistically isotropic hydrometeors such as tumbling hail. Whereas K_{dp} is a good indicator of rain if rainfall rates are relatively large (>20 mm h^{-1}; section 4b), it is not uniquely related to median size. (Rather, it is more closely related to content.) We choose thresholds of K_{dp} in Table 6 to be nearly compatible with values of Z_h, which, in turn, are compatible with Z_{dr}. This choosing is done by matching the rain rates in the Marshall–Palmer Z, R relation with the K_{dp}, R relation (Sachidananda and Zrnić 1987). Because K_{dp} depends on mass contents and the presence of oriented hydrometeors and is relatively insensitive to details of size distributions, the above procedure generally is very accurate except, perhaps, in regions where rain and mixed-phase hydrometeors coexist. It has been shown by Balakrishnan and Zrnić (1990a), for example, that ice and mixed-phase hydrometeors might occur to the left, and pure rain to the right, of the curve given by

$$Z_h(K_{dp}) = 8\ \log K_{dp} + 49 \quad (\text{dB}Z). \tag{7}$$

In practice, the observed value of Z_h can be compared with that from Eq. (7) [used to obtain Eq. (3)]. Pure rain is likely if $Z_h < Z_h(K_{dp})$ from the Z_h, K_{dp} curve given by Eq. (7). A pure hail or a rain/hail mixture is possible if $Z_h > Z_h(K_{dp})$. The rain region in the Z_h, K_{dp} parameter space (Fig. 4a) is in general accord with the work presented by Ryzhkov and Zrnić (1996) and Eq. (7). Last, the fraction of ice from K_{dp} should be $F_{ik} < 0.25$ for pure rain (Table 6).

Recently, Hubbert et al. (1998) found an indication of water drops with sizes as large as 2 mm and a mode of about $D \approx 1$ mm in regions near the freezing level and close to the updraft of a severe hailstorm. Loney et al. (1999) confirmed this signature using radar and in situ aircraft data. Based on research by Rasmussen (1984) and Rasmussen and Heymsfield (1987), Hubbert et al. (1998) hypothesize that these drops are shed from melting or growing hailstones in a column near the updraft. Such regions are associated with enhanced values of K_{dp} (0.5° to 1.5° km^{-1}), thus the term "K_{dp} column." Values of other PR variables in the K_{dp} column include $50 < Z_h < 60$ dBZ, $0 < Z_{dr} < 2$ dB, $-22 < \text{LDR}_{vh} < -16$ dB, and $0.94 < |\rho_{hv}(0)| < 0.96$ (Hubbert et al. 1998). The values for PR variables defining the K_{dp} column are included in Table 6, and the parameter space associated with Z_h, K_{dp} pairs is shown in Fig. 4b. Values of Z_h, Z_{dr} pairs associated with the K_{dp} column are presented in Fig. 2b.

6) BACKSCATTER DIFFERENTIAL PHASE

For 10-cm wavelength radar, maximum raindrop sizes (≈8 mm) should produce barely measurable δ (Balakrishnan and Zrnić 1990b). The values of $|\delta| < 1°$ in Table 6 accommodate small statistical uncertainty. In contrast, it has been suggested recently that frozen or freezing drops might be associated with $|\delta| > 1°$ (Hubbert et al. 1998).

7) LINEAR DEPOLARIZATION RATIO

The lowest values of LDR_{vh} (<−32 dB) can indicate small, nearly spherical raindrops ($D < 1$ mm). Slightly larger values of LDR_{vh} (−27 to −34 dB) are found in more intense rain, whereas values of $\text{LDR}_{vh} > -27$ dB might be produced by large, deformed, or canted drops (Bringi et al. 1986a). The largest values of LDR_{vh} in pure rain should be about −24 dB (Bringi et al. 1986a). These values are based upon observations with 3-cm-wavelength radar. Interestingly, they basically agree with observations presented by Hendry et al. (1987), valid at a 1.82-cm wavelength, and work presented by Frost et al. (1989, 1991) for 10-cm-wavelength radar. Based on previous work described above, that done by Frost et al. (1989, 1991) at a 10-cm wavelength, and recent observations with the CSU-CHILL radar (e.g., Carey and Rutledge 1998; Hubbert et al. 1998), we suggest $\text{LDR}_{vh} < -25$ dB in Table 6 as the upper bound

TABLE 6. Thresholds for some variables to identify rain. Note: Large drops in low concentration, Z_{dr} column, K_{dp} column, and LDR_{vh} cap are not considered in the general category of rain.

Rain	Z_h (dBZ)	Z_{dr} (dB)	$\lvert\rho_{hv}(0)\rvert$ (%)	K_{dp} (° km^{-1})	LDR_{vh} (dB)	δ (°)	F_{ik} (%)	F_{iz} (%)	H_{dr}	K_{dr}	T (K)
Rain	<60	>0	>0.95	>0	< −25	$\lvert\delta\rvert < 1$	<0.25	<0.25	<0	<1	>263.15
$D_o < 1$ mm	<28	0–0.7	>0.97	0–0.03	< −32	$\lvert\delta\rvert < 1$	<0.25	<0.25	<0	<1	>273.15
$1 < D_o < 2$ mm	28–44	0.7–2	>0.95	0.03–0.6	−34 to −28	$\lvert\delta\rvert < 1$	<0.25	<0.25	<0	<1	>268.15
$D_o > 2$ mm	44–60	>2	>0.95	>0.6	−30 to −25	$\lvert\delta\rvert < 1$	<0.25	<0.25	<0	<1	>263.15
$D_o > 3$ mm (large drops—low concentration)	5–35	>3	>0.95	>0	> −25	$\lvert\delta\rvert < 15$	<0.25	<0.25	<0	<1	>263.15
Z_{dr} column (drops growing by coalescence)	30–45	1–5	>0.95	0–0.5	> −25	$\lvert\delta\rvert < 15$	<0.25	<0.25	<0	<1	>263.15
K_{dp} column (drops shed from hail)	50–60	0–2	0.94–0.96	0.5–1.5	−22 to −16	—	<0.25	<0.25	<0	<1	<273.15
LDR_{vh} cap (frozen and freezing drops)	40–60	0–2	0.92–0.96	0–1	−25 to −19	—	—	—	<0	<1	<273.15

for rain. Recall that our thresholds are not ''hard'' but can be exceeded, albeit with confidence less than 0.5. The confidence for pure rain identification should be increased if the threshold ranges for Z_h, LDR_{vh} pairs are both satisfied (Fig. 5).

d. Rain–wet hail mixtures and mixed-phase hydrometeors

Thresholds for some of the variables in Table 7 for rain–wet hail mixture are largely compatible with the thresholds for rain (Table 6) and/or hail (Table 2). The rain–small wet hail mixture should also be considered to be valid for rain–melting graupel mixtures common in the U.S. High Plains. Note that thresholds for Z_h, LDR_{vh}, H_{dr}, K_{dr}, and δ for rain–wet hail are nearly identical to thresholds for hail.

1) REFLECTIVITY

The values for Z_h are consistent with those for wet hail.

2) DIFFERENTIAL REFLECTIVITY

In general, mixtures of larger raindrops and small, water-coated hailstones contribute to positive Z_{dr}, whereas the presence of larger hail tends to reduce Z_{dr} (Table 7). For small hail mixed with rain, we set the upper threshold to 6 dB, which is about 7 dB lower than the maximum values for a model of a melting hailstone 12 mm in diameter (Aydin and Zhao 1990) and is about 0.5 dB higher than similar scattering-model results of Vivekanandan et al. (1990) for a 10-mm hailstone. Extreme Z_{dr} of 5 and 6 dB might indicate very large water drops with ice cores [ice particles that are melting or experiencing wet growth as defined by Pruppacher and Klett (1981) or Young (1993)], because often a torus of liquid water forms about the equator of a small hailstone ($D < 9$ mm), making it more oblate [and stabilizing tumbling motions (Rasmussen et al. 1984; Rasmussen and Heymsfield 1987)]. Large melting or wet hailstones ($D > 20$ mm) tend to have smaller Z_{dr}, because they cannot support a torus of water around their equators. We, therefore, reduce the upper thresholds by 2 or 3 dB per hail size category (Table 7) and adjust the lower thresholds slightly upward from values for pure hail. Figure 2a shows the Z_h, Z_{dr} pairs associated with rain–wet hail mixtures, with larger values for Z_{dr} than those for pure hail. The values for rain–wet hail mixtures are in general agreement with observations and measurements described by Carey and Rutledge (1998) and Hubbert et al. (1998), though our upper thresholds for Z_{dr} are larger than those of Carey and Rutledge. The accommodation for melting graupel mixed with rain (incorporated in the rain–small wet hail category) is based on recent observations presented by Hubbert et al. (1998).

TABLE 7. Thresholds for some variables to classify rain–wet hail mixtures.

Rain–wet hail	Z_h (dBZ)	Z_{dr} (dB)	$\lvert\rho_{hv}(0)\rvert$ (%)	K_{dp} (° km^{-1})	LDR$_{vh}$ (dB)	δ (°)	F_{ik} (%)	F_{iz} (%)	H_{dr}	K_{dr}	T (K)
Rain–wet hail	45–80	−1 to 6	<0.95	>0	>−25	$\lvert\delta\rvert > 1$	0.25–0.75	0.25–0.75	>1	>2	>263.15
Rain–small wet hail	45–60	−0.5 to 6	<0.95	>0	>−25	$\lvert\delta\rvert < 15$	0.25–0.75	0.25–0.75	5–33	>2	>268.15
Rain–large wet hail	55–65	−0.5 to 3	<0.92	>0	>−22	$5 < \lvert\delta\rvert < 15$	0.25–0.75	0.25–0.75	18–38	>4	>263.15
Rain–giant wet hail	60–80	−1 to 1	<0.88	>0	>−18	$15 < \lvert\delta\rvert < 30$	0.25–0.75	0.25–0.75	>23	>8	>263.15

3) REFLECTIVITY DIFFERENCE AND HAIL SIGNAL

The fraction of ice from Z_{dp} should range from $0.25 < F_{iz} < 0.75$ (Table 7). The values for differential reflectivity hail signal are consistent with those for wet hail. Use of H_{dr} for rain–wet hail is similar to that for wet hail.

4) CORRELATION COEFFICIENT

Balakrishnan and Zrnić (1990b) suggest that $\lvert\rho_{hv}(0)\rvert$ can be as low as or lower than 0.90 in rain–hail mixtures. For two hydrometeor types in a resolution volume, $\lvert\rho_{hv}(0)\rvert$ is a minimum when the contribution to the echo power by one type is close to the contribution by the other type (Jameson 1989; Balakrishnan and Zrnić 1990b; Aydin and Zhao 1990). In rain–hail mixtures, $\lvert\rho_{hv}(0)\rvert$ decreases toward ground because of increasing rain amounts and, therefore, hydrometeor diversity below the melting level. This trend is nearly monotonic when the size and number of hailstones is significant; when not the case, $\lvert\rho_{hv}(0)\rvert$ reaches a minimum and starts to increase as hailstones melt into rain. Zrnić et al. (1993a) found that $\lvert\rho_{hv}(0)\rvert < 0.94$ and $Z_{dr} < -0.5$ for rain–hail mixtures, with hail sizes of $20 < D < 50$ mm. These findings, as well as recent measurements with both the Cimarron and CSU-CHILL radars (Hubbert et al. 1998), are used to define the thresholds in Table 7. Regions where the Z_h, $\lvert\rho_{hv}(0)\rvert$ pairs correspond to rain–wet hail mixtures are depicted in Fig. 3.

5) SPECIFIC DIFFERENTIAL PHASE

As described in the section for hail, the presence of hail should have a negligible influence on K_{dp}. In heavy rain, K_{dp} can be appreciably larger than zero, as seen in Table 4 and Fig. 4a. Therefore, these thresholds are also entered in Table 7. A small ice core ($D < 9$ mm) surrounded by a liquid torus might appear as a large water drop. Thus, large populations of these mixed-phase particles can produce large values of K_{dp}. Figure 4a shows Z_h, K_{dp} pairs for rain–wet hail mixtures to indicate enhanced classification confidence. The fraction of ice from K_{dp} should be $0.25 < F_{ik} < 0.75$ (Table 7).

6) BACKSCATTER DIFFERENTIAL PHASE

Values of δ for rain–wet hail mixtures are consistent with those for wet hail as described in the section on hail.

7) LINEAR DEPOLARIZATION RATIO

For rain–wet hail mixtures, LDR$_{vh}$ should be similar to or slightly smaller than that for pure wet hail, with larger values of LDR$_{vh}$ for larger hail sizes. Carey and Rutledge (1998) indicate LDR$_{vh}$ values for rain–hail mixtures that are slightly smaller than those for pure hail at 10-cm wavelength, as does Holler et al. (1994) for 5-cm wavelength. We employ this trend in Table 7 and Fig. 5.

Some recent, interesting observations of LDR$_{vh}$ include caps ($-25 <$ LDR$_{vh}$ < -19 dB) on top of Z_{dr} columns. In these columns, Z_{dr} is large (up to about 5 dB), and $\lvert\rho_{hv}(0)\rvert$ is smaller than expected in pure rain. The LDR$_{vh}$ caps also are associated with reduced values of $\lvert\rho_{hv}(0)\rvert$, and K_{dp} typically is between 0° and 1° km^{-1}. Jameson et al. (1996) and Hubbert et al. (1995, 1998) attribute these sets of observations to zones of freezing or frozen drops. Hubbert et al. (1995, 1998) provide modeling support for this hypothesis. The threshold values for the PR variables from Hubbert et al. (1998) for LDR$_{vh}$ caps are provided in Table 6. The parameter space where Z_{dr}, LDR$_{vh}$ pairs satisfy the thresholds (Fig. 5) strengthens the confidence in the identification of LDR$_{vh}$ caps. Values of Z_h, K_{dp} pairs as well as values of Z_h, Z_{dr} pairs associated with LDR$_{vh}$ caps also are plotted in Fig. 2b and Fig. 4b, respectively, to show when increased confidence in these measurements might be valid. More modeling studies and in situ observations are needed to help to verify these values.

e. Snow crystals and aggregates

Whereas PR data and, possibly, the temperature of the environmental air can be used to identify snow aggregates, classification of crystal types at 10-cm-wavelength radar is still in need of much research. One of the problems is that ice crystal types are difficult to discern because the dielectric constant for ice crystals

and snow aggregates is dependent on particle density (which can be strongly size dependent); therefore, low-density particles produce lower contrasts among the PR variables. Small crystal sizes also can reduce magnitudes of PR signatures. Furthermore, ice crystals have a large variety of shapes that are difficult to model. Nevertheless, much recent work has been done, particularly for 3-cm-and-shorter-wavelength radar for Rayleigh scatterers that is of relevance (e.g., Matrosov 1992; Aydin and Tang 1997; Vivekanandan and Adams 1993; Vivekanandan et al. 1993a, 1994; Atlas et al. 1995; Gosset et al. 1995; Matrosov et al. 1996; Reinking et al. 1997). There also has been some work done at 10-cm wavelength (e.g., Thomason et al. 1995; Ryzhkov and Zrnić 1998a; Ryzhkov et al. 1998). Of particular interest is that low-density crystals that are within the limit of validity of the Rayleigh–Gans approximation exhibit little or no polarization dependence on Z_h even if they have very complex shapes (Matrosov 1992). Nevertheless, we constructed Table 8 on the basis of available model results and observational measurements with 10-cm-wavelength radar and modification of information of Rayleigh-regime results from shorter-wavelength radar (which would be at least qualitatively consistent with Rayleigh-regime information from longer-wavelength radar).

The density of snow crystals and aggregates varies as a function of habit from 50 to 900 kg m^{-3}, with higher values expected for solid ice structures and wetted particles. The size distributions of ice crystals and snow aggregates can be represented by exponential and gamma functions, and the total number of concentrations is on the order of 1–10^4 m^{-3} for aggregates, 10–10^9 m^{-3} for individual crystals at colder temperatures ($T < -20$°C), and often as high as 10^4 m^{-3} at warmer temperatures (Pruppacher and Klett 1981). The size of large aggregates can be $D \approx 20$–50 mm, whereas the size of large crystals can be $D \approx 1$–5 mm. The shapes of aggregates are approximately spherical to extremely oblate, and the approximate shapes of crystals can vary from extreme prolates and oblates to essentially spheres (Pruppacher and Klett 1981). Most individual crystals tend to fall with their largest dimension horizontally oriented unless there are pronounced electric fields. Aggregates also can fall in a horizontally oriented manner or may tumble. A summary of crystal densities and size relations is presented in Table 9. Radar signatures of ice crystals are sensitive to their mean canting angle (Vivekanandan et al. 1993a).

TABLE 8. Thresholds for some variables to classify snow crystals and aggregates.

Snow–crystals		Z_h (dBZ)	Z_{dr} (dB)	$\lvert\rho_{hv}(0)\rvert$ (%)	K_{dp} (° km^{-1})	LDR_{vh} (dB)	δ (°)	T (K)
Snow–crystals		<45	−0.5 to 6	>0.95 (0.5 to 0.9 wet)	−0.6 to 1	<−20 (<−10 wet)	—	
Snow aggregate	Dry	<35	0–1	>0.95	0–0.2	<−25	—	<273.15
	Wet	<45	0.5–3	0.5–0.9	0–0.5	−10 to −20	$-5 < \delta < 10$	>273.15
Crystals (dry)	Vertical	<35	−0.5 to 0.5	>0.95	−0.6 to 0	<−24	—	<273.15
	Horizontal	<35	0–6	>0.95	0–0.6	<−27	—	<273.15
	Habit	<35	2–6	>0.95	0–0.6	<−28	—	<273.15
	Plate–dendrite	<35	1–4	>0.95	0–0.6	<−30	—	<273.15
	Column–thick plate	<35	0–3	>0.95	0–0.6	<−27	—	<273.15
	Needle–sheath	<35						

1) REFLECTIVITY FACTOR

Measured Z_h (or Z_v) of snow aggregates and crystals is generally smaller than for most other precipitating hydrometeors except, perhaps, drizzle largely because of low dielectric effects, regardless of any of the possible crystal shapes. Moreover, Z_h is highly dependent on particle density (densities of aggregates typically are

much lower than those for crystals as shown in Table 9; also see references listed above). Boucher and Wieler (1985) report a range of 10–36 dBZ. Ohtake and Henmi (1970) computed Z_h from size distribution data and concluded that larger aggregates of dendrites produce the largest Z_h. The five crystal forms considered by Ohtake and Henmi give a maximum of $Z_h < 35$ dBZ, which agrees with the results of Ryzhkov et al. (1998) and Ryzhkov and Zrnić (1998a). Thus, we set an upper threshold for dry snow at 35 dBZ. Wetting could increase the reflectivity by 5–10 dBZ or so, from increased particle density and increased dielectric constant as suggested by observations and models (Zrnić et al. 1993a; Vivekanandan et al. 1993; Ryzhkov et al. 1998; Ryzhkov and Zrnić 1998a; among others). In addition, Z_h can be enhanced for wet snow, because these particles can grow to larger sizes through more efficient aggregation in association with wet ice surfaces. Moreover, PR signatures of aggregates can be enhanced as they collapse into raindrops. All of these aspects associated with aggregates can lead to melting-level brightband signatures in the Z_h fields (as well as in other PR fields). Hence, the upper threshold of $Z_h \approx 45$ dBZ is valid for wet aggregates. Vertical gradients in Z_h at and below the melting level can be useful in discriminating between aggregates and graupel. The lack of a prominent bright band (gradient yet to be specified) can be useful in indicating graupel when there are warm surface temperatures. Moreover, the lack of any bright band can be useful in indicating snow when temperatures through a column are all below the freezing point of water.

2) DIFFERENTIAL REFLECTIVITY

In general, it is difficult at best to discriminate snow aggregates and crystal types with Z_{dr}, let alone any of the other PR variables. One reason is there are but very few known relations between physical particle attributes and the very complicated scattering characteristics of aggregates and crystals. Another is the unknown index of refraction, which depends on particle density and on which Z_{dr} depends. Nevertheless, it has been found in some instances that Z_{dr} might be used to identify aggregates, needles, columns, and plates under ideal conditions (e.g., Vivekanandan et al. 1993; Brandes et al. 1995). Individual crystals have large axis ratios and generally fall with a horizontal orientation, which would produce positive Z_{dr}. For 5-cm-wavelength radar, Meischner et al. (1991a,b) suggest that Z_{dr} of 2–5 dB might be associated with pristine dendrites or aggregates composed of 5–6 crystals, and that Z_{dr} of 0–0.5 might be associated with larger dendrites and aggregates. The lower values for dry aggregates take into account that they may be 1) small, 2) of low density, 3) associated with low dielectric constants, 4) nearly spherical, and/or 5) tumbling while falling. A scattering model of oriented oblate spheroids with densities of snow produces Z_{dr} less than 1 dB (Illingworth et al. 1987), which is the upper limit for dry snow aggregates in Table 8. For wet aggregates, measured values of Z_{dr} at the bottom of the melting layer range from 1 dB (Zrnić et al. 1993a; Moninger et al. 1984) to 2.5 dB (Hagen et al. 1993). Recent measurements of Z_{dr} up to 4 dB (CSU-CHILL radar) have been ascribed to snow aggregates. There are not many scattering model results or observations yet of scattering by columns (or thick plates), plates (or sectors and dendrites), or needles (or sheaths) at a 10-cm wavelength. Geometric considerations dictate that, of these three crystal forms, plates have the largest Z_{dr}, and needles have the lowest Z_{dr}. We use information available for a 10-cm wavelength (Vivekanandan et al. 1993; Vivekanandan 1994) and extrapolate results from an 8-mm wavelength (Evans and Vivekanandan 1990; Vivekanandan and Adams 1993) to estimate the range of thresholds provided in Table 8. The largest dimensions considered by Evans and Vivekanandan are 2 mm, which is in the resonance region of scattering and causes large excursions of Z_{dr}. The upper thresholds in Table 8 are smaller by about 2 dB from the model results, because at a 10-cm wavelength, resonance effects generally are not present in ice crystals.

In summary, $0.4 < Z_{dr} < 3.0$ dB with $30 < Z_h < 45$ dBZ may indicate wet snow at warmer temperatures, whereas $0.4 < Z_{dr} < 3.0$ dB with $5 < Z_h < 30$ dBZ may indicate pristine ice crystals or lightly aggregated crystals at colder temperatures. At cold temperatures, measurements of $0 < Z_{dr} < 0.2$ dB with $5 < Z_h < 30$ dBZ could be indicative of dry aggregates. In addition, values of Z_{dr} and Z_h that are similar to those for aggregates in the melting layers might be indicative of the rain–snow line as seen in some Oklahoma winter storms (Ryzhkov et al. 1998; Ryzhkov and Zrnić 1998a). These values are incorporated into Table 8 and in Fig. 2b. Below the melting level, as aggregates collapse into drops, measurements of Z_{dr} typically show a decrease. Further decreases in Z_{dr} from 1 to 2 km below the melting layer could be associated with drops breaking up into smaller particles from collisions with each other.

It should be noted that bulk interpretations of aggregates and crystals might be misleading. For example, Bader et al. (1987) found that a few large, low-density aggregates could produce low bulk values of Z_{dr} that could conceal high values of Z_{dr} possible from many numerous, small needles and columns when the aggregates and crystals are mixed.

3) REFLECTIVITY DIFFERENCE AND HAIL SIGNAL

A few investigators have used Z_{dp} implicitly to separate rain from frozen hydrometeors and for quantification of ice amounts (e.g., Golestani et al. 1989; Conway and Zrnić 1993; Ryzhkov et al. 1998). It has not been widely accepted for identification of specific ice hydrometeor types, however. The most detailed example possibly is that by Meischner et al. (1991a), who had a 5-cm-wavelength radar and in situ measurements. At

TABLE 9. Equations and parameters for snow crystals and aggregates.

Parameter	Equations	Reference
Distribution	$n(D) = n_o \exp(-D\lambda)$ (m^{-4}) exponential distribution $n(D) = n_o D^{\mu} \exp(-D\lambda)$ (m^{-4}) gamma distribution	Lin et al. (1983), Ferrier (1994), and Harrington et al. (1995)
Total number	$N_t = n_o \lambda^{-1}$ (m^{-3}) exponential distribution $N_t = n_o \lambda^{-(1+\mu)} \Gamma(1 + \mu)$ (m^{-3}) gamma distribution	Lin et al. (1983) and Ferrier (1994)
Slope	$\lambda = [(\rho n_o \pi)/(\rho_{air} q)]^{-1/4}$ (m^{-1}) exponential distribution $\lambda = \{[\Gamma(4 + \mu)\rho N_t \pi]/[6\Gamma(1 + \mu)\rho_{air} q]\}^{-1/3}$ (m^{-1}) gamma distribution	Lin et al. (1983), Ferrier (1994), and Harrington et al. (1995)
Intercept	$n_o = 4 \times 10^4$ (m^{-4}) exponential distribution $n_o = N_t \lambda^{-(1+\mu)} [\Gamma(1 + \mu)]^{-1}$ ($m^{-(4+\mu)}$) gamma distribution	Lin et al. (1983), Hauser and Ameyanc (1986), Ferrier (1994), and Harrington et al. (1995)
Median diam (D_o) and mass-weighted mean diam (D_m) or diameter or length–mass	Exponential distribution $D_o = 3.67\lambda^{-1}$ (m); $D_m = 4\lambda^{-1}$ (m) spherical aggregate Gamma distribution $D_o = (3.67 + \mu)\lambda^{-1}$ (m); $D_m = [\Gamma(5 + \mu)/\Gamma(4 + \mu)]\lambda^{-1}$ (m) spherical aggregate Others (mass and lengths in SI units) $L = 0.1871M^{0.3429}$ (m) (bullet–column, $L/D < 2$, $10 < L < 1000$ μm) $D = 1.634M^{0.4141}$ (m) (dendrite, $10 < D < 90$ μm) $D = 9.780M^{0.4890}$ (m) (dendrite, $90 < D < 1000$ μm) $L = 0.1871M^{0.3429}$ (m) (column, $L/D < 2$, $10 < L < 1000$ μm) $L = 0.2693M^{0.3591}$ (m) (hollow column, $L/D < 2$, $10 < L < 50$ μm) $L = 0.2856M^{0.3617}$ (m) (hollow column, $L/D < 2$, $50 < L < 1000$ μm) $L = 0.3491M^{0.3503}$ (m) (needle–sheath–column, $L/D > 2$, $10 < L < 1000$ μm) $D = 1.188M^{0.4040}$ (m) (plate—thin, $10 < D < 3000$ μm) $D = 1.576M^{0.4141}$ (m) (sector–stellar broad branch, $10 < D < 100$ μm) $D = 4.882M^{0.4598}$ (m) (sector–stellar broad branch, $100 < D < 1000$ μm)	Auer and Veal (1970), Davis and Auer (1974), Doviak and Zrnić (1993), Jayaweera and Cottis (1969), Mason (1994), Mango and Lee (1966), Mitchell et al. (1990), Mitchell (1994), and Pruppacher and Klett (1981)
Height; length–diameter	Spherical to oblate (aggregate) $D = 0.4764L^{0.958}$ (m) (bullet–column, $L/D < 2$) $H = 6.734 \times 10^{-4} D^{0.4150}$ (m) (dendrite) $D = 0.4764L^{0.958}$ (m) (column, $L/D < 2$) $D = 0.2566L^{0.892}$ (m) (hollow column, $L/D < 2$) $D = 0.1858L^{0.927}$ (m) (needle–sheath–column, $L/D > 2$) $H = 1.250 \times 10^{-4} D^{0.4740}$ (m) (plate—thin) $H = 6.734 \times 10^{-4} D^{0.4150}$ (m) (sector–stellar broad branch)	References above
Density–diameter or length	$\rho = 0.4417D^{-1.1}$ (kg m^{-3}) (aggregate) $\rho = 0.9464D^{-0.6}$ (kg m^{-3}) (aggregate) $\rho\max = 100D^{0.0}$ (kg m^{-3}) (aggregate) $\rho = 759.8L^{-0.0038}$ (kg m^{-3}) (bullet–column, $L/D < 2$) $\rho = 43.49D^{-0.377}$ (kg m^{-3}) (dendrite) $\rho = 769.8L^{-0.0141}$ (kg m^{-3}) (column, $L/D < 2$) $\rho = 345.5L^{-0.0915}$ (kg m^{-3}) (hollow column, $L/D < 2$) $\rho = 300.0L^{0.0}$ (kg m^{-3}) (needle–sheath–column, $L/D > 2$) $\rho = 900.0D^{0.0}$ (kg m^{-3}) (plate—thin) $\rho = 43.49D^{-0.01410}$ (kg m^{-3}) (sector–stellar broad branch)	Heymsfield (1972), Mason (1994), and Mitchell (1994)
Fall velocity*	$V = 0.81Z_h^{0.017}$ (m s^{-1}) (aggregates) $V = 4.836D^{0.25}$ (m s^{-1}) (aggregates) $V = 49\,422.0L^{1.415}$ (m s^{-1}) (bullet–column, $L/D > 2$) $V = 43.55D^{0.748}$ (m s^{-1}) (dendrite) $V = 49\,422.0L^{1.415}$ (m s^{-1}) (column, $L/D < 2$) $V = 49\,422.0L^{1.415}$ (m s^{-1}) (hollow column, $L/D < 2$) $V = 1008.0L^{1.309}$ (m s^{-1}) (needle–sheath–column, $L/D > 2$) $V = 131.6.0D^{0.824}$ (m s^{-1}) (plate—thin) $V = 43.55D^{0.748}$ (m s^{-1}) (sector–stellar broad branch)	Churchill and Houze (1984), Davis and Auer (1974), Heymsfield (1972), Jayaweera and Cottis (1969), and Lin et al. (1983)

TABLE 9. Continued.

Parameter	Equations	Reference
Shape (approximate)	Spherical to oblate (aggregates) Prolate spheroid (bullet–column, $L/D < 2$) Disk (dendrite) Prolate spheroid (column, $L/D < 2$) Prolate spheroid (hollow column, $L/D < 2$) Extreme prolate spheroid (needle–sheath–column, $L/D > 2$) Disk (plate) Disk (sector–stellar broad branch)	Lin et al. (1983), Pruppacher and Klett (1981), Mango and Lee (1966), and references above for crystal types and aggregates
Orientation	Horizontally oriented with some oscillation; vertically oriented small crystals in electric fields	List and Schemenauer (1971), Pruppacher and Klett (1981), and Caylor and Illingworth (1996)
Rate	$R = 3.6 \times 10^6\, M\rho V$ (mm h^{-1}) (can be used in general with M, ρ, and V)	Churchill and Houze (1984)
Content*	$M = 8.0 \times 10^{-3}\, Z_h^{0.605}$ (kg m^{-3}) $M = 0.034 Z_h^{0.40}$ (g m^{-3}) (aggregates) $M = 0.035 Z_h^{0.51}$ (g m^{-3}) (ice from stratiform) $M = 0.088 Z_h^{0.58}$ (g m^{-3}) (ice from cirrus) $M = 3K_{dp}$ $M(K_{dp}) = 3.22K_{dp}$ (crystals and lightly aggregated crystals) $M(K_{dp}, Z_{dr}) = 0.48K_{dp}[1 - 10^{-0.1Z_{dr}}]$	Churchill and Houze (1984), Thomason (1995), Heymsfield (1977), Atlas et al. (1995), Vivekanandan et al. (1994), Ryzhkov and Zrnić (1995), and Ryzhkov et al. (1998)
Dielectric constant	$(\epsilon - 1)(\epsilon + 2)^{-1}$ $\approx (\rho\rho_i^{-1})(\epsilon_i - 1)/(\epsilon_i + 2)^{-1}$ $\epsilon = 1.33 - 8.09j$: ice with $\rho = 200$ (kg m^{-3}) $\epsilon = 1.97 - 2.71j$: ice with $\rho = 500$ (kg m^{-3}) $\epsilon = 2.78 - 6.12j$: ice with $\rho = 800$ (kg m^{-3}) $\epsilon = 3.1699 - 0.003975j$: ice with $\rho = 900$ (kg m^{-3}) at 0°C	Aydin and Zhao (1990), Vivekanadan (1993a), Ryzhkov et al. (1998), and Matrosov et al. (1996)

* Z_h (mm^6 m^{-3}); q is mixing ratio (kg kg^{-1}); ρ is hydrometeor density (kg m^{-3}); Γ is the complete gamma function; for spheres unless indicated.

this time, we are not confident that Z_{dp} (at 10-cm wavelength) can indicate crystal type. Also, H_{dr} has not been used to indicate crystals or aggregates.

4) CORRELATION COEFFICIENT

Values of $|\rho_{hv}(0)|$ in pure snow are similar to those for rain if there is little variation in the canting angles of snow crystals (e.g., Balakrishnan and Zrnić 1990b). Observations by Illingworth and Caylor (1989) indicate $|\rho_{hv}(0)|$ that are as low as 0.60 in the bright band associated with melting aggregates. Values this low also have been seen regularly with the Cimarron radar in Oklahoma (e.g., Ryzhkov et al. 1998). It also has been demonstrated observationally and theoretically that $|\rho_{hv}(0)|$ decreases substantially in regions of mixed-phase hydrometeors at the bottom of the melting zone where snow aggregates begin to collapse into raindrops (e.g., Zrnić et al. 1993a, 1994; Ryzhkov and Zrnić 1998a; Ryzhkov et al. 1998). These considerations lead us to suggest a range of $0.50 < |\rho_{hv}(0)| < 0.90$ for wet aggregates, a lower threshold of 0.95 for dry aggregates, and a lower threshold of 0.95 for other types of snow particles. Confidence in the wet snow aggregate category should be enhanced if both $30 < Z_h < 45$ dBZ and $0.50 < |\rho_{hv}(0)| < 0.90$ are satisfied (Fig. 3; Ryzhkov et al. 1998; Ryzhkov and Zrnić 1998a).

5) SPECIFIC DIFFERENTIAL PHASE

Attempts have been made to use K_{dp} to identify crystal habits. Hendry et al. (1976) suggest that K_{dp} should be larger for dendrites than for aggregates and recorded 0.36° km^{-1} associated with snow. More recently Golestani et al. (1989) noted K_{dp} of 0.75° km^{-1} in oriented crystals that possibly were mixed with some aggregate. (The aggregates were not assumed to contribute significantly to K_{dp}.) In addition, K_{dp} measurements in a storm anvil ranged from 0.25° to 0.5° km^{-1} (Vivekanandan et al. 1994). These measurements were attributed to horizontally aligned crystals in a mixture with effectively spherical aggregates. Observations with CSU-CHILL radar and scattering-model results suggest that K_{dp} might increase when crystal density increases. These observations are consistent with values modeled by Vivekanandan et al. (1994) and Evans and Vivekanandan (1990), which, for example, predict $K_{dp} \approx 0.25°$ km^{-1} for snow. Vivekanandan and Adams (1993) show PR scattering-model results at an 8-mm wavelength for various elevation angles between 0° and 90° that suggest some habit discrimination with K_{dp}, as well as with other PR variables; however, this possibility needs to be tested at 10-cm wavelength. Recent observations with the Cimarron radar and an instrumented T-28 aircraft suggest the presence of horizontal crystals if $0.0° < K_{dp} < 0.6°$ km^{-1} and $5 < Z_h < 30$ dBZ. In addition, vertically ori-

ented crystals are indicated if $0.0° > K_{dp} > -0.6°$ km^{-1} and $5 < Z_h < 30$ dBZ in electric fields (Ryzhkov and Zrnić 1998a; Ryzhkov et al. 1998), as presented in Table 8 and Fig. 4b. These values are valid for $T < 0$°C. Carey and Rutledge (1998) also suggest $K_{dp} < -0.25°$ km^{-1} and $Z_h < 40$ dBZ for vertically aligned crystals in electric fields, which concurs with Ryzhkov et al.'s values. Wet aggregates in the melting layer can produce $K_{dp} \approx 0.5°$–$1°$ km^{-1} (Zrnić et al. 1993a), which can help to discriminate dry from wet aggregates, with wet aggregates producing the large phase shift. Last, Ryzhkov and Zrnić (1998a) found that K_{dp} in snow is almost always larger at a fixed value of Z_h than that observed in rain. In Table 8, K_{dp} is not used to discriminate among columns, plates, and needles, as suggested by the 8-mm-wavelength results of Vivekanandan and Adams (1993). Extrapolation to 10-cm wavelength is possible because the absence of resonance effects (at 10-cm wavelength) can only reduce discriminating properties present at shorter wavelengths. The small positive thresholds ($K_{dp} > 0.0°$ km^{-1}) indicate a general trend in ϕ_{dp} caused by the presence of numerous horizontally oriented particles. Vertically oriented crystals also are taken into account in Table 8 and Fig. 4b; the orientation is due to the presence of strong electric fields that can align small crystals. Whereas K_{dp} is sensitive to electric fields because many small crystals can be reoriented, Z_{dr} generally is not sensitive to electric fields because less numerous but larger crystals probably cannot be reoriented (Ryzhkov et al. 1998).

6) Backscatter differential phase

Of all the crystal and snow forms, only large wet aggregates are known to produce measurable δ. At a 10-cm wavelength, aggregates might produce δ when sizes exceed $D \approx 10$ mm. The range $-5° < \delta < 10°$ in Table 8 is obtained from a scattering model and observational measurements (Zrnić et al. 1993a).

7) Linear depolarization ratio

Values of LDR_{vh} between -29 and -26 dB have been observed in association with dry, moderately heavy snow at a wavelength of 1.82 cm (Hendry et al. 1987). Hendry et al. also noted an LDR_{vh} bright band near the melting level in precipitation. Similarly, Frost et al. (1991) measured $\mathrm{LDR}_{vh} > -22$ dB in the bright band at a 10-cm wavelength. They report more moderate values of $-6 < \mathrm{LDR}_{vh} < -22$ dB in dry ice regions, however. Scattering-model results of LDR_{vh} for aggregates at 10-cm wavelength are between -25 and -20 dB (Vivekanandan et al. 1993a), though much smaller values were produced by the scattering model of Frost et al. (1989). Matrosov (1991) suggests that there might be some crystal discrimination possibility with LDR_{vh} but that the signal differences are weak. His results showed that plates and needles produce the largest LDR_{vh} signals ($\mathrm{LDR}_{vh} \approx -27$ to -28 dB, respectively), and that thick plates, solid columns, and bullets produce the smallest ($\mathrm{LDR}_{vh} \approx -30$ to -31 dB, respectively). Recent wintertime observations with the CSU-CHILL and S-POL radars agree, in general, with the larger observed values described, especially near the melting level. The thresholds in Table 8 and Fig. 5 are approximately valid for a 10-cm wavelength and are based on some of the observations described above and on the scattering-model results from Matrosov (1991), Vivekanandan and Adams (1993), and Vivekanandan et al. (1993a, 1994). Note that electric fields that align small ice crystals into the vertical prior to lightning discharges have been shown to increase, reduce, and not affect LDR_{vh} signatures (Caylor and Chandrasekar 1996). Therefore, LDR_{vh} is not used to indicate vertically aligned crystals in electric fields. The possibility to study storm electrification and lightning location with dual-polarimetric radar has begun to gain acceptance in the meteorology community in the past five yr or so.

Table 10. Hydrometeor types using Z_h and T.

Basic hydrometeor types		
Species	Z_h (dBZ)	T (K)
Rain (100%)	<50	>273.15
Rain–small hail (75/25%)	50–55	>273.15
Rain–hail (50/50%)	55–60	>273.15
Rain–hail (25/75%)	>60	>273.15
Hail	>50	<263.15
Hail	>60	>273.15
Graupel	35–50	<273.15
Snow	<35	<273.15

f. Case where Z_h and T are the only variables available

If Z_h is the only radar variable available, then, with the addition of temperature, some general information for hydrometeor identification could be extracted by eliminating physically unrealistic possibilities (Table 10). Ambiguities are impossible to avoid with just Z_h and T.

4. Estimating precipitation amounts

For as long as weather radar has existed, there have been attempts made to use Z_h to quantify how much precipitation is falling, often in conjunction with statistical procedures. Over the past two decades, PR has emerged as a very useful remote sensing instrument for estimating precipitation amounts, with most improvements for rain amount estimation.

For correct quantitative estimation of precipitation amounts and other parameters, the type of contributing

hydrometeor needs to be determined, as described in section 3. Determining hydrometeor amounts is significantly more difficult than hydrometeor classification. In this section, we suggest some quantitative estimates for D_o, terminal velocity V, R, ice or liquid water content M, and total number concentration N_t. These estimates depend on assumptions about the size distributions, axis ratios a/b, particle densities ρ, fall orientations, shapes, dielectric constants for water, etc. The accuracy of these estimates depends on the type and amount of hydrometeors and on the availability, resolution, reliability, and accuracy of the PR data. The information for the quantitative estimation is put forward in Tables 1, 3, 5, and 9 for use in scattering and cloud modeling (with references provided for more detailed explanation). For brevity, the discussion in the remainder of this section is limited to estimation of precipitation rates and contents.

To transform the PR data into quantitative precipitation estimates, equations described in previously published studies are employed. Many of these equations were obtained from model simulations of realistic size distributions, whereas others were determined from in situ measurements. Some precipitation types, such as rain, can be quantified from two or more fundamentally different relations. Then, consistency among precipitation amounts can be used to check the estimate.

Quantification of ice hydrometeors is complicated by the presence of hydrometeors that are themselves mixed phase, as well as by mixed–hydrometeor phase populations. For most of the ice species, amount estimates rely heavily on the reflectivity factor. When ice is mixed with rain, the liquid contribution to Z_h often can be removed by careful use of some of the PR variables. Recently, some precipitation amount estimates for ice using $K_{\rm dp}$ have been developed (section 4e). For quantifying amounts for all ice habits, however, there is still much work to be done. We submit, though, that, at the very least, if the classification is correct, then the quantification based on the reflectivity factor alone, with all its uncertainties, might be more reliable. The quantitative precipitation estimate equations for the previously described variables, including hail, graupel, rain, and snow crystals are summarized in Tables 1, 3, 5, and 9, respectively. A brief discussion of each follows.

a. Hail amounts

Estimates of hail content and size are crude at best (Table 1), and the errors could be significant, depending on how much the actual size distribution deviates from the assumed distribution. The Cheng and English (1983) hail size distribution has gained some acceptance and is suggested, at least, for the present. The exponent and concentration of the distribution are related, and therefore the exponent is a function of Z_h alone.

b. Rain amounts

Whereas natural hydrometeor size distributions are highly variable, approximations with a three-parameter gamma function might be adequate for most applications (Ulbrich 1983); we urge caution, however, because exceptions commonly occur. If Z_h is the only variable, then the Marshall and Palmer (1948) distribution (Table 5) and semiempirical relations can be used to determine rainfall rates. In the WSR-88D system (Table 5), Z_h is truncated at 51 dBZ for arid and semiarid regions to prevent contamination by hail (Vieux and Bedient 1998). In maritime, tropical, and other precipitation systems, truncation should be at 55 dBZ (Vieux and Bedient 1998; Aydin et al. 1995). Care must be taken with $R(Z)$ estimates, even at 10-cm wavelengths, for various reasons, including attenuation (Ryzhkov and Zrnić 1995c). However, $R(Z)$ relations can be tuned to some extent with PR variables (Ryzhkov and Zrnić 1997). In addition, multidimensional Z_h properties (gradients, horizontal and vertical morphology, precipitation system type, etc.) might be used to improve $R(Z)$ estimates and identify the Z_h ''bright band'' (Rosenfeld et al. 1995a,b) based on objective classification of precipitation system type.

Rain rate estimates using Z_h and $Z_{\rm dr}$ are based on several assumptions, including 1) drops fall with their minor axis vertically oriented, 2) axis ratios and size relations are known, and 3) drops exhibit little canting in the mean. In addition, the assumptions that the raindrop size distribution is exponential and that $D_{\rm max}$ is reasonably large are also made. The $R(Z_h, Z_{\rm dr})$ for rainfall rate in Table 5 was developed by Sachidananda and Zrnić (1987). A similar relation for M is also in Table 5. Chandrasekar et al. (1990) note that $R(Z_h, Z_{\rm dr})$ formulations outperform $R(Z)$ relations. Other similar relations for R and M using Z_h and Z_v have been proposed by Chandrasekar et al. (1990), Aydin and Giridhar (1992), and Gorgucci et al. (1993), among many others.

Sachidananda and Zrnić (1987) and Steinhorn and Zrnić (1988) proposed that R for rain can be estimated using $K_{\rm dp}$ from 10-cm-wavelength radar (Table 5). Similar $R(K_{\rm dp})$ and $M(K_{\rm dp})$ relations also are proposed by Aydin and Giridhar (1992), Chandrasekar et al. (1990), Gorgucci et al. (1993, 1995), Aydin et al. (1995), and Ryzhkov and Zrnić (1995, 1996a,b), and are partially summarized by Brandes et al. (1997). Note that R and M are nearly linearly dependent on $K_{\rm dp}$. More recently, $R(Z_{\rm dr}, K_{\rm dp})$ relations have been proposed (Jameson 1991; Aydin et al. 1995; Ryzhkov and Zrnić 1995a, 1996b). A summary of a number of R and M relations for various PR variable combinations is presented in Table 5.

Studies by Sachidananda and Zrnić (1987), Balakrishnan and Zrnić (1990a), and Chandrasekar et al. (1990) suggest an $R(Z)$ relation for $R < 20$ mm h^{-1}, $R(Z_h, Z_v)$ for $20 < R < 50$ mm h^{-1}, and $R(K_{\rm dp})$ for $R > 50$ mm h^{-1} (Table 5). Note that Chandrasekar et al. (1990) use a 70 mm h^{-1} threshold for $R(K_{\rm dp})$. The small-

er value we suggest capitalizes on the other advantageous properties of K_{dp} rather than just statistical errors of estimates; these values follow recommendations by Sachidananda and Zrnić (1987). More recently, Ryzhkov and Zrnić (1996) recommend one $R(K_{dp})$ relation for all rain-rate regimes but with longer range averaging intervals for smaller rain rates.

Errors resulting from drop size distribution variations and statistical uncertainty, under ideal conditions, [simulations with gamma distribution and Pruppacher and Beard (1970) axis ratios] are 30%–40% for $R < 20$ mm h^{-1}, 20%–30% for $20 < R < 60$ mm h^{-1}, and better than 20% for $R > 60$ mm h^{-1} (Chandrasekar et al. 1990; Sachidananda and Zrnić 1987; Balakrishnan et al. 1989). Recent findings suggest accumulation errors with $R(K_{dp})$ between 10% and 20% (Aydin et al. 1995; Ryzhkov and Zrnić 1995a; Ryzhkov and Zrnić 1996b). Errors for $R(Z_{dr}, K_{dp})$ estimates are similar to, or slightly better than, those for $R(K_{dp})$ (Ryzhkov and Zrnić 1995a).

c. Rain–wet hail mixture amounts

Because K_{dp} is almost unaffected by the presence of hail, it is probably the most suitable PR variable to estimate the amount of liquid water content in rain–ice mixtures (e.g., Aydin et al. 1995). After Balakrishnan and Zrnić (1990a), $Z_{hr} = 24\,800\,K_{dp}^{1.386}$, where Z_{hr} is the reflectivity ($mm^6\ m^{-3}$) from rain. Aydin and Giridhar (1992) also proposed a similar rain curve using K_{dp} at a 5-cm wavelength. The contribution of ice to the reflectivity is simply $Z_{hi} = Z - Z_{hr}$. Golestani et al. (1989) suggest that the reflectivity difference [(Eq. A4)] can be applied to separate the amounts of rain and hail in a mixture of the two. In pure rain, tightly correlated pairs of Z_{dp} and Z_{hr} lie along a well-defined line given by Eq. (2). Significant lateral displacement (2dB) of the data from this line is indicative of mixed phase or hail and is caused by the reflectivity of ice Z_{hi}.

The fraction of ice contribution F_i to Z_h in ice and liquid mixtures is computed as $F_{im} = Z_{hi}(Z_{hi} + Z_{hr})^{-1}$, where Z_{hi} and Z_{hr} are in units of $mm^6\ m^{-3}$, and the subscript m refers to the method of computing rain amount (F_{iz} is from Z_{dp} and F_{ik} is from K_{dp}). If K_{dp} is used to estimate the rain amounts in the mixture, the errors are comparable to those in pure rain. For estimates from Z_{dp}, errors are at least as large as in pure rain. If both K_{dp} and Z_{dp} are available, it probably is better to compute the liquid and frozen fractions from K_{dp} because the measurement of the liquid part is more robust (Balakrishnan and Zrnić 1990b).

d. Graupel–small hail amounts

There is a paucity of data concerning quantitative relations for graupel–small hail. Part of the problem is a nonexistence of well-defined relations between PR variables and parameters of the size distribution. For lack of better estimates, we list Hauser and Amayenc's (1986) formulation using Z_h for low-density (150 km m^{-3}) lump graupel (Table 3). We suggest that estimates for R and M for high-density graupel–small hail follow those for hail (e.g., Table 1). Errors in the graupel rate and content calculations are uncertain.

e. Snow crystals and aggregate amounts

Radar estimates of ice water content of crystals and aggregates are greatly complicated by the multitude of crystal sizes and shapes, various crystal and aggregate densities, and dielectric constants, among others. Estimates of snow amounts have been made from Z_h [e.g., Sekhon and Srivastava 1970; Heymsfield 1977 (stratiform); Herzegh and Hobbs 1980; Smith 1984; Sassen 1987; Matrosov 1992; Detwiler et al. 1993 (crystals); Atlas et al. 1995 (cirrus); Aydin and Tang 1997; Thomason et al. 1995; Matrosov 1998]. Some of these relations are in Table 9. Vivekanandan et al. (1993a, 1994) relate ice contents for crystals as a function of density and shape to K_{dp} and Z_{dp}; these relations might be used for columns, plates, and needles (Table 9). More recently, Ryzhkov and Zrnić (1995) and Ryzhkov et al. (1998) used K_{dp} and combined Z_{dr} and K_{dp} to estimate ice water contents for crystals and lightly aggregated snowflakes (Table 9). Of the PR variables, K_{dp} and Z_{dp} might be the most useful, because they are more sensitive to number concentration (especially K_{dp}) than to shape. An ice water content from Z_{dr} (or Z_{dp}) and K_{dp} also might be of value, because it probably is insensitive to crystal shape and density. Of all the snow types, the determination of the amount of wet aggregates is probably the most difficult. Still needed are reliable estimates of errors in R and M for snow.

5. Summary

The results of numerous modeling and observational studies have been synthesized into relations between PR variables and hydrometeor types. These relations are expressed as threshold boundaries in multidimensional PR variable spaces meant for deducing bulk hydrometeor types, which subsequently permits the quantification of hydrometeor amounts. On a PR variable threshold boundary or on the edge of a multidimensional PR variable space, our confidence or belief of a correct hydrometeor identification is suggested to be 0.5 on a scale from 0 to 1. Therefore, the boundaries and spaces are suitable for use in fuzzy classification and similar algorithms. Relations to determine the amounts and average sizes of classified hydrometeors are tabulated succinctly. At present, we consider these relations to be some of the more reliable estimates. A better understanding of PR variables through comparison with observations and models will improve these relations. A fuzzy classifier algorithm that also quantifies precipitation amounts will be described in a subsequent paper and is considered to be versatile in that it accepts any

of the available PR variables. Researchers interested in the determination of bulk qualitative or quantitative hydrometeor properties throughout a PR sample volume might find the synthesized information herein useful either for testing similar or for developing alternative procedures.

Acknowledgments. Partial funding for this research was provided by the National Science Foundation grants ATM-9120009, ATM-9311911, EAR-9512145, and ATM-9617318; the National Severe Storms Laboratory; the Cooperative Institute for Mesoscale Meteorological Studies; and the Graduate College of the University of Oklahoma (Dr. E. C. Smith). Conversations over the past five years with Drs. V. Bringi, A. Detwiler, R. Doviak, K. Emanuel, M. Fritsch, R. Gall, J. Keeler, S. Lasher-Trapp, D. Lilly, R. Maddox, S. Nelson, E. Rasmussen, P. Smith, J. Vivekanadan, and J. Wurman, and the support of Drs. K. Droegemeier, F. Carr, and P. Lamb are gratefully acknowledged. We thank Messrs. M. Askelson and B. Gordon and Ms. Y. Liu for fruitful discussions and for editing radar data. Ms. K. Kanak is thanked for the tremendous amount of time she invested in helping to critique, to organize, and to edit this paper. Ms. Nichole Peltier is acknowledged for helping with some of the literature search.

APPENDIX

Polarimetric Radar Variables

Reflectivity factor (Battan 1973; horizontal polarization; backscatter variable):

$$Z_h = (4\lambda^4/\pi^4|K_w|^2)\langle|s_{hh}|^2\rangle. \quad \text{(A1)}$$

Reflectivity factor (vertical polarization; backscatter variable):

$$Z_v = (4\lambda^4/\pi^4|K_w|^2)\langle|s_{vv}|^2\rangle. \quad \text{(A2)}$$

Differential reflectivity (Seliga and Bringi 1976; backscatter variable):

$$Z_{\rm dr} = 10\ \log(\langle|s_{hh}|^2\rangle/\langle|s_{vv}|^2\rangle). \quad \text{(A3)}$$

Reflectivity difference (Golestani et al. 1989; backscatter variable):

$$Z_{\rm dp} = 10\ \log(Z_h - Z_v), \qquad \text{for } Z_h > Z_v. \quad \text{(A4)}$$

Differential phase shift (propagation variable):

$$\phi_{\rm dp} = \phi_{hh} - \phi_{vv}. \quad \text{(A5)}$$

Specific differential phase (propagation variable):

$$K_{\rm dp} = [\phi_{\rm dp}(r_2) - \phi_{\rm dp}(r_1)]\ [2(r_2 - r_1)]^{-1}. \quad \text{(A6)}$$

Correlation coefficient at zero lag (Sachidananda and Zrnić 1985; backscatter variable):

$$|\rho_{hv}(0)| = \langle s_{vv}s_{hh}^*\rangle/(\langle s_{hh}^2\rangle^{1/2}\langle s_{vv}^2\rangle^{1/2}). \quad \text{(A7)}$$

Linear depolarization ratio (backscatter variable):

$$\text{LDR}_{vh} = 10\ \log(\langle|s_{vh}|^2\rangle/\langle|s_{hh}|^2\rangle). \quad \text{(A8)}$$

Two additional backscatter variables are the complex correlations between copolar and cross-polar voltages; however, they are not discussed here because it is not known how useful the information they provide is (Doviak and Zrnić 1993). In addition, attenuation and depolarization from propagation are difficult to measure, and their use is limited; thus they are not discussed. In this appendix, s_{ij} refers to an element of the backscattering matrix of a hydrometeor (Zrnić 1991). The first subscript i indicates the polarization of the backscattered field [horizontal h or vertical v], and the second subscript j refers to the polarization of the incident field; $K_w = (\epsilon_w - 1)/(\epsilon_w + 2)$ is a factor related to the dielectric constant of water; ϵ_w is the dielectric constant; λ is radar wavelength; ϕ_{hh} and ϕ_{vv} are the phases of the horizontally polarized and vertically polarized waves; and r_1 and r_2 are the distances of measurements 1 and 2 from a radar. The brackets $\langle\ \rangle$ indicate expectations expressed in terms of the distribution of mean hydrometeor properties such as size, shape, shape irregularities, fall orientation, canting angle, particle density, composition, dielectric constant, and others.

REFERENCES

Al-Khatib, H. N., T. A. Seliga, and V. N. Bringi, 1979: Differential reflectivity and its use in the radar measurements of rainfall. Ohio State University Atmos. Sci. Prog. Rep. AS-S-106, 131 pp.

Askelson, M. A., J. M. Straka, and D. S. Zrnić, 1997: A study of the kinematics and microphysical evolution of a supercell from first echo using polarization diversity radar. Preprints, *28th Int. Conf. on Radar Meteorology,* Austin, TX, Amer. Meteor. Soc., 9–10.

——, ——, and ——, 1998: Kinematical and microphysical evolution of the 22 June 1995 storm. Preprints, *19th Conf. on Severe Local Storms,* Minneapolis, MN, Amer. Meteor. Soc., 56–59.

Atlas, D., S. Y. Matrosov, A. J. Heymsfield, M.-D. Chou, and D. B. Wolff, 1995: Radar and radiation properties of ice clouds. *J. Appl. Meteor.,* **34,** 2329–2345.

Auer, A. H., and P. L. Veal, 1970: The dimensions of ice crystals in natural clouds. *J. Atmos. Sci.,* **27,** 919–926.

Aydin, K., and T. A. Seliga, 1984: Radar polarimetric backscattering properties of conical graupel. *J. Atmos. Sci.,* **41,** 1887–1892.

——, and Y. Zhao, 1990: A computational study of polarimetric radar observables in hail. *IEEE Trans. Geosci. Remote Sens.,* **28,** 412–421.

——, and V. Giridhar, 1992: C-band dual polarization radar observables in rain. *J. Atmos. Oceanic Technol.,* **9,** 383–390.

——, and D. S. Zrnić, 1992: Modeling polarimetric signatures of precipitation. *Appl. Comp. Electrom. Soc.,* **7,** 22–25.

——, and C. Tang, 1997: Relationships between IWC and polarimetric measurands at 94 and 220 GHz for hexagonal columns and plates. *J. Atmos. Oceanic Technol.,* **14,** 1055–1063.

——, T. A. Seliga, and V. N. Bringi, 1984: Differential radar scattering properties of model hail and mixed phase hydrometeors. *Radio Sci.,* **19,** 58–66.

——, Y. M. Lure, and T. A. Seliga, 1986a: Polarimetric radar measurements of rainfall compared with ground-based rain gauges during MAYPOL '84. *IEEE Trans. Geosci. Remote Sens.,* **28,** 412–422.

——, T. A. Seliga, and V. Balaji, 1986b: Remote sensing of hail with a dual linear polarization radar. *J. Climate Appl. Meteor.,* **25,** 1475–1484.

——, Y. Zhao, and T. A. Seliga, 1990: A differential reflectivity radar

hail measurement technique: Observations during the Denver hailstorm of 13 June 1984. *J. Atmos. Oceanic Technol.,* **7,** 104–113.

——, T. M. Walsh, and D. S. Zrnić, 1993: Analysis of the dual-polarization radar and T-28 aircraft mesurements during an Oklahoma hailstorm. Preprints, *26th Int. Conf. on Radar Meteorology,* Norman, OK, Amer. Meteor. Soc., 540–542.

——, V. N. Bringi, and L. Liu, 1995: Rain-rate estimation in the presence of hail using S-band specific differential phase and other radar parameters. *J. Appl. Meteor.,* **34,** 404–410.

Bader, M. J., S. A. Clough, and G. P. Fox, 1987: Aircraft and dual polarization radar observations of hydrometeors in light stratiform precipitation. *Quart. J. Roy. Meteor. Soc.,* **113,** 491–515.

Balakrishnan, N., and D. S. Zrnić, 1990a: Estimation of rain and hail rates in mixed-phase precipitation. *J. Atmos. Sci.,* **47,** 565–583.

——, and ——, 1990b: Use of polarization to characterize precipitation and discriminate large hail. *J. Atmos. Sci.,* **47,** 1525–1540.

——, ——, J. Goldhirsh, and J. Rowland, 1989: Comparison of simulated rain rates from disdrometer data employing polarimetric radar algorithms. *J. Atmos. Oceanic Technol.,* **6,** 476–486.

Barge, B. L., and G. A. Isaac, 1973: The shape of Alberta hailstones. *J. Rech. Atmos.,* **7,** 11–20.

Battan, L. J., 1973: *Radar Observation of the Atmosphere.* University of Chicago Press, 323 pp.

Beard, K. V., and A. R. Jameson, 1983: Raindrop canting. *J. Atmos. Sci.,* **40,** 448–454.

——, and J. Q. Feng, 1991: A perturbation model of raindrop oscillation characteristics with aerodynamic effects. *J. Atmos. Sci.,* **48,** 1856–1868.

——, R. J. Kubesh, and H. T. Ochs III, 1991: Laboratory measurements of small drop distortion. Part I: Axis ratios and fall behavior. *J. Atmos. Sci.,* **48,** 698–710.

Blackman, M., and A. J. Illingworth, 1993: Differential phase measurement of precipitation. Preprints, *26th Int. Conf. on Radar Meteorology,* Norman, OK, Amer. Meteor. Soc., 745–747.

Bluestein, H. B., 1992: *Synoptic–Dynamic Meteorology in Midlatitudes.* Oxford University Press, 431 pp.

Boucher, R. J., and J. G. Wieler, 1985: Radar determination of snowfall rate and accumulation. *J. Appl. Meteor.,* **24,** 68–73.

Brandes, E. A., C. Kessinger, J. D. Tuttle, and J. Vivekanandan, 1993: An evaluation of multiparameter radar measurements for detecting hail. Preprints, *26th Int. Conf. on Radar Meteorology,* Norman, OK, Amer. Meteor. Soc., 522–524.

——, J. Vivekanandan, J. D. Tuttle, and C. J. Kessinger, 1995: A study of thunderstorm microphysics with multiparameter radar and aircraft observations. *Mon. Wea. Rev.,* **123,** 3129–3143.

——, ——, and J. W. Wilson, 1997: Radar rainfall estimates of the Buffalo Creek flash flood using WSR-88D and polarimetric radar data. Preprints, *28th Conf. on Radar Meteorology,* Austin, TX, Amer. Meteor. Soc., 123–124.

Bringi, V. N., T. A. Seliga, and W. A. Cooper, 1984: Analysis of aircraft hydrometeor spectra and differential reflectivity (ZDR) radar measurements during the Cooperative Convective Precipitation Experiment. *Radio Sci.,* **19,** 157–167.

——, R. M. Rasmussen, and J. Vivekanandan, 1986a: Multiparameter radar measurements in Colorado convective storms. Part I: Graupel melting studies. *J. Atmos. Sci.,* **43,** 2545–2563.

——, J. Vivekanandan, and J. D. Tuttle, 1986b: Multiparameter radar measurements in Colorado convective storms. Part II: Hail detection studies. *J. Atmos. Sci.,* **43,** 2564–2577.

——, D. A. Burrows, and S. M. Menon, 1991: Multiparameter radar and aircraft study of raindrop spectral evolution in warm-based clouds. *J. Appl. Meteor.,* **30,** 853–880.

——, D. Brunkow, V. Chandrasekar, S. Ruthledge, P. Kennedy, and A. Mudukutore, 1993: Polarimetric measurements in Colorado convective storms using the CSU-CHILL radar. Preprints, *26th Int. Conf. on Radar Meteorology,* Norman, OK, Amer. Meteor. Soc., 519–521.

——, L. Liu, P. C. Kennedy, V. Chandrasekar, and S. A. Rutledge, 1996: Dual multiparameter radar observations of intense convective storms: The 24 June 1992 case study. *Meteor. Atmos. Phys.,* **59,** 3–31.

——, K. Knupp, A. Detwiler, L. Liu, I. J. Caylor, and R. A. Black, 1997: Evolution of a Florida thunderstorm during the Convection and Precipitation/Electrification experiment: The case of 9 August 1991. *Mon. Wea. Rev.,* **125,** 2131–2159.

——, V. Chandrasekar, and X. Rongrui, 1998: Raindrop axis ratios and size distributions in Florida rainshafts: An assessment of multiparameter radar algorithms. *IEEE Trans. Geosci. Remote Sens.,* **36,** 703–715.

Carey, L. D., and S. A. Rutledge, 1998: Electrical and multiparameter radar observations of a severe hailstorm. *J. Geophys. Res.,* **103,** 13 979–14 000.

Caylor, I. J., and V. Chandrasekar, 1996: Time-varying ice crystal orientation in thunderstorms observed with multiparameter radar. *IEEE Trans. Geosci. Remote Sens.,* **34,** 847–858.

Chandrasekar, V., V. N. Bringi, N. Balakrishnan, and D. S. Zrnić, 1990: Error structure of multiparameter radar and surface measurements of rainfall. Part III: Specific differential phase. *J. Atmos. Oceanic Technol.,* **7,** 621–629.

Cheng, L., and M. English, 1983: A relationship between hailstone concentration and size. *J. Atmos. Sci.,* **40,** 204–213.

Churchill, D. D., and R. A. Houze Jr., 1984: Mesoscale updraft magnitude and cloud-ice content from the ice budget of the stratiform region of a tropical cloud cluster. *J. Atmos. Sci.,* **41,** 1717–1725.

Conway, J. W., and D. S. Zrnić, 1993: A study of embryo production and hail growth using dual-Doppler and multiparameter radars. *Mon. Wea. Rev.,* **121,** 2512–2528.

Davis, C. I., and A. H. Auer Jr., 1974: Use of isolated orographic clouds to establish the accuracy of diffusional ice crystal growth equations. Preprints, *Conf. on Cloud Physics,* Tucson, AZ, Amer. Meteor. Soc., 141–147.

Detwiler, A. G., N. C. Knight, and A. J. Heymsfield, 1993: Magnitude of error factors in estimates of snow-particle masses from images. *J. Appl. Meteor.,* **32,** 804–809.

Doviak, R. J., and D. S. Zrnić, 1993: *Doppler Radar and Weather Observations.* Academic Press, 562 pp.

——, V. Bringi, A. Ryzhkov, A. Zahrai, and D. S. Zrnić, 2000: Considerations for polarimetric upgrades to operational WSR-88D radars. *J. Atmos. Oceanic Technol.,* **17,** 257–278.

Evans, K. F., and J. Vivekanandan, 1990: Multiparameter radar and microwave radiative transfer modeling of nonspherical atmospheric ice particles. *IEEE Trans. Geosci. Remote Sens.,* **28,** 423–437.

Ferrier, B. S., 1994: A double-moment multiple-phase four-class bulk ice scheme. Part I: Description. *J. Atmos. Sci.,* **51,** 249–280.

Frank, W. M., and C. Cohen, 1987: Simulation of tropical convective systems. Part I: A cumulus parameterization. *J. Atmos. Sci.,* **44,** 3787–3799.

Fritsch, J. M., and Coauthors, 1998: Quantitative precipitation forecasting: Report on the eighth prospectus development team, U.S. Weather Research Program. *Bull. Amer. Meteor. Soc.,* **79,** 285–299.

Frost, I. R., A. J. Illingworth, and I. J. Caylor, 1989: Aircraft and polarization radar measurements of a triggered lightning event. *Proc. Int. Lightning and Static Electricity Conf.,* 1A.1.1–1A.1.4.

——, J. W. F. Goddard, and A. J. Illingworth, 1991: Hydrometeor identification using cross polar radar measurements and aircraft verification. Preprints, *25th Int. Conf. on Radar Meteorology,* Paris, France, Amer. Meteor. Soc., 658–661.

Fulton, R., and G. M. Heymsfield, 1991: Microphysical and radiative characteristics of convective clouds during COHMEX. *J. Appl. Meteor.,* **30,** 98–116.

Galati, G., and G. Pavan, 1995: Computer simulation of weather radar signals. *Simul. Pract. Theory,* **3,** 17–44.

Gal-Chen, T., 1978: A method for initialization of the anelastic equations: Implications for matching models with observations. *Mon. Wea. Rev.,* **106,** 587–606.

Goddard, J. W. F., S. M. Cherry, and V. N. Bringi, 1982: Comparison

of dual-polarization radar measurements of rain with ground-based disdrometer measurements. *J. Appl. Meteor.,* **21,** 252–256.
Golestani, Y., V. Chandrasekar, and V. N. Bringi, 1989: Intercomparison of multiparameter radar measurements. Preprints, *24th Conf. on Radar Meteorology,* Tallahassee, FL, Amer. Meteor. Soc., 309–314.
Gorgucci, E., G. Scarchilli, and V. Chandrasekar, 1993: A robust pointwise estimator of rainfall rate and liquid water content using polarization diversity radar. Preprints, *26th Int. Conf. on Radar Meteorology,* Norman, OK, Amer. Meteor. Soc., 777–779.
——, V. Chandrasekar, and G. Scarchilli, 1995: Radar and surface measurement of rainfall during CaPE: 26 July 1991 case study. *J. Appl. Meteor.,* **34,** 1570–1577.
Gosset, M. E. J., A. J. Illingworth, P. R. A. Brown, and J. W. G. Thomason, 1995: The effect of ice crystal density assumption in inferring reflectivity vs ice content relationship. Preprints, *27th Conf. on Radar Meteorology,* Vail, CO, Amer. Meteor. Soc., 547–549.
Gunn, R., and G. D. Kinzer, 1949: The terminal velocity of fall for water droplets in stagnant air. *J. Meteor.,* **6,** 243–248.
Hagen, M., J. Hubbert, C. Richter, V. N. Bringi, and P. Meischner, 1993: Bright band observations with radar and aircraft. Preprints, *26th Int. Conf. on Radar Meteorology,* Norman, OK, Amer. Meteor. Soc., 304–305.
Hall, M. P. M., S. M. Cherry, J. W. Goddard, and G. R. Kennedy, 1980: Raindrop sizes and rainfall rate measured by dual-polarization radar. *Nature,* **285,** 195–198.
——, J. W. F. Goddard, and S. M. Cherry, 1984: Identification of hydrometeors and other targets by dual-polarization radar. *Radio Sci.,* **19,** 132–140.
Harrington, J. L., M. P. Meyers, R. L. Walko, and W. R. Cotton, 1995: Parameterization of ice crystal conversion in cirrus clouds using double moment basis functions. *J. Atmos. Sci.,* **52,** 4344–4366.
Hauser, D., and P. Ameyanc, 1986: Retrieval of cloud water and water vapor contents from Doppler radar data in a tropical squall line: Application to the case of a tropical squall line. *J. Atmos. Sci.,* **43,** 823–838.
Hendry, A., G. C. McCormick, and L. G. Barge, 1976: Ku-band and S-band observations of differential propagation constant in snow. *IEEE Trans. Antennas Propag.,* **AP-24,** 521–525.
——, Y. M. M. Antar, and G. C. McCormick, 1987: On the relationship between the degree of preferred orientation in precipitation and dual-polarization radar echo characteristics. *Radio Sci.,* **22,** 37–50.
Herzegh, P. H., and P. V. Hobbs, 1980: The mesoscale and microscale structure and organization of clouds and precipitation in midlatitude cyclones. II: Warm-frontal clouds. *J. Atmos. Sci.,* **37,** 597–611.
——, and A. R. Jameson, 1992: Observing precipitation through dual-polarization radar measurements. *Bull. Amer. Meteor. Soc.,* **73,** 1365–1374.
Heymsfield, A. J., 1972: Ice crystal terminal velocities. *J. Atmos. Sci.,* **29,** 1348–1357.
——, 1977: Precipitation development in stratiform ice clouds: A microphysical and dynamical study. *J. Atmos. Sci.,* **34,** 367–381.
Holler, H., V. N. Bringi, J. Hubbert, M. Hagen, and P. F. Meischner, 1994: Life cycle and precipitation formation in a hybrid-type hailstorm revealed by polarimetric and Doppler radar measurements. *J. Atmos. Sci.,* **51,** 2500–2522.
Hubbert, J. V., and V. N. Bringi, 1995: An iterative filtering technique for the analysis of copolar differential phase and dual-frequency radar measurements. *J. Atmos. Oceanic Technol.,* **12,** 643–648.
——, and ——, 1997: The effects of 3-body scattering on differential reflectivity. Preprints, *28th Conf. on Radar Meteorology,* Austin, TX, Amer. Meteor. Soc., 11–12.
——, V. Chandrasekar, V. N. Bringi, and P. Meischner, 1993a: Processing and interpretation of coherent dual-polarized radar measurements. *J. Atmos. Oceanic Technol.,* **10,** 155–164.
——, V. N. Bringi, H. Holler, M. Hagen, and P. Meischner, 1993b: Examples of polarimetric C-band radar measurements from convective storms during CLEOPATRA. Preprints, *26th Int. Conf. on Radar Meteorology,* Norman, OK, Amer. Meteor. Soc., 528–529.
——, ——, ——, and P. Meischner, 1995: C-band polarimetric signatures from a convective storm during CLEOPATRA. Preprints, *27th Conf. on Radar Meteorology,* Vail, CO, Amer. Meteor. Soc., 443–445.
——, ——, and L. D. Carey, 1998: CSU-CHILL polarimetric radar measurements from a severe hail storm in Eastern Colorado. *J. Appl. Meteor.,* **37,** 749–775.
Husson, D., and Y. Pointin, 1989: Quantitative estimation of the hail fall intensity with a dual polarization radar and a hailpad network. Preprints, *24th Conf. on Radar Meteorology,* Tallahassee, FL, Amer. Meteor. Soc., 318–321.
Illingworth, A. J., 1988: The formation of rain in convective clouds. *Nature,* **336,** 754–756.
——, and I. J. Caylor, 1986: Detection of hail by dual-polarization radar. *Nature,* **320,** 431–433.
——, and ——, 1989: Cross-polar observation of the bright band. Preprints, *24th Conf. on Radar Meteorology,* Tallahassee, FL, Amer. Meteor. Soc., 323–327.
——, and ——, 1991: Copolar correlation measurements of precipitation. Preprints, *25th Int. Conf. on Radar Meteorology,* Paris, France, Amer. Meteor. Soc., 650–653.
——, and D. S. Zrnić, 1995: Workshop on weather radar polarimetry for research and operational applications. *Bull. Amer. Meteor. Soc.,* **76,** 555–558.
——, J. W. F. Goddard, and S. M. Cherry, 1986: Detection of hail by dual-polarization radar. *Nature,* **320,** 431–433.
——, ——, and ——, 1987: Polarization radar studies of precipitation development in convective storms. *Quart. J. Roy. Meteor. Soc.,* **113,** 469–489.
Jameson, A. R., 1985: On deducing the microphysical character of precipitation from multiple-parameter radar polarization measurements. *J. Climate Appl. Meteor.,* **24,** 1037–1047.
——, 1989: The interpretation and meteorological application of radar backscatter amplitude ratios at linear polarizations. *J. Atmos. Oceanic Technol.,* **6,** 908–919.
——, 1991: A comparison of microwave techniques for measuring rainfall. *J. Appl. Meteor.,* **30,** 32–50.
——, and K. V. Beard, 1982: Raindrop axial ratios. *J. Appl. Meteor.,* **21,** 257–259.
——, and J. H. Davé, 1988: An interpretation of circular polarization measurements affected by propagation differential phase shift. *J. Atmos. Oceanic Technol.,* **5,** 405–415.
——, M. J. Murphy, and E. P. Krider, 1996: Multiple-parameter radar observations of isolated Florida thunderstorms during the onset of electrification. *J. Appl. Meteor.,* **35,** 343–354.
Jayaweera, K. O. L. F., and R. E. Cottis, 1969: Fall velocities of plate-like and columnar ice crystals. *Quart. J. Roy. Meteor. Soc.,* **95,** 703–709.
Jones, D. M., 1959: The shape of raindrops. *J. Atmos. Sci.,* **16,** 504–510.
Joss, J., and I. Zawadzki, 1997: Raindrop distributions again? Preprints, *28th Conf. on Radar Meteorology,* Austin, TX, Amer. Meteor. Soc., 326–327.
Keenan, T., K. Glasson, F. Cummings, T. S. Bird, J. Keeler, and J. Lutz, 1998: The BMRC/NCAR C-band polarimeteric (C-POL) radar system. *J. Atmos. Oceanic Technol.,* **15,** 871–886.
Kennedy, P. C., S. A. Rutledge, and V. N. Bringi, 1997: Hail precursor signatures observed in multiparameter radar data. Preprints, *28th Conf. on Radar Meteorology,* Austin, TX, Amer. Meteor. Soc., 51–52.
Kessler, E., 1969: *On the Distribution and Continuity of Water Substance in Atmospheric Circulation. Meteor. Monogr.,* No. 32, Amer. Meteor. Soc., 84 pp.
Knight, C. A., and N. C. Knight, 1970: The falling behavior of hailstones. *J. Atmos. Sci.,* **27,** 672–681.
Knight, N. C., 1986: Hailstone shape factor and its relation to radar interpretation of hail. *J. Climate Appl. Meteor.,* **25,** 1956–1958.

Kry, P. R., and R. List, 1974: Angular motions of freely falling spheroidal hailstone models. *Phys. Fluids,* **17,** 1093–1102.

Leitao, M. J., and P. A. Watson, 1984: Application of dual linearly polarized radar data to prediction of microwave path attenuation at 10–30 GHz. *Radio Sci.,* **19,** 209–221.

Lemon, L. R., 1998: The radar ''Three-body scatter spike'': An operational large-hail signature. *Wea. Forecasting,* **13,** 327–340.

Lin, Y.-L., R. D. Farley, and H. D. Orville, 1983: Bulk parameterization of the snow field in a cloud model. *J. Climate Appl. Meteor.,* **22,** 1065–1092.

Lipshutz, R. C., J. F. Pratte, and J. R. Smart, 1986: An operational ZDR-based precipitation type/intensity product. Preprints, *23d Conf. on Radar Meteorology,* Snowmass, CO, Amer. Meteor. Soc., JP91–JP94.

List, R., 1986: Properties and growth of hailstones. *Thunderstorm Dynamics and Morphology,* E. Kessler, Ed., University of Oklahoma Press, 259–276.

——, and R. S. Schemenauer, 1971: Free-fall behavior of planar snow crystals, conical graupel and small hail. *J. Atmos. Sci.,* **28,** 110–115.

——, U. W. Rentsch, A. C. Byram, and E. P. Lozowski, 1973: On the aerodynamics of spheroidal hailstone models. *J. Atmos. Sci.,* **30,** 653–661.

Liu, L., V. N. Bringi, I. J. Caylor, and V. Chandrasekar, 1993: Intercomparison of multiparameter radar signatures from Florida storms. Preprints, *26th Int. Conf. on Radar Meteorology,* Norman, OK, Amer. Meteor. Soc., 733–735.

Locatelli, J. D., and P. V. Hobbs, 1974: Fall speeds and masses of solid precipitation particles. *J. Geophys. Res.,* **79,** 2185–2197.

Lohmeier, S. P., S. M. Sekelsky, J. M. Firda, G. A. Sadowy, and R. E. McIntosh, 1997: Classification of particles in stratiform clouds using the 33 and 95 GHz polarimetric Cloud Profiling Radar System (CPRS). *IEEE Trans. Geosci. Remote Sens.,* **35,** 256–258.

Loney, M. L., D. S. Zrnić, A. V. Ryzhkov, and J. M. Straka, 1999: In situ and multiparameter radar observations of an isolated Oklahoma supercell at far range. Preprints, *29th Int. Conf. on Radar Meteorology,* Montreal, PQ, Canada, Amer. Meteor. Soc., 188–191.

Longtin, D. R., C. F. Bohren, and L. J. Battan 1987: Radar backscattering by large, spongy ice oblate spheroids. *J. Atmos. Oceanic Technol.,* **4,** 355–358.

Lopez, R. E., and J. P. Aubagnac, 1997: The lightning activity of a hailstorm as a function of changes in its microphysical characteristics inferred from polarimetric radar observations. *J. Geophys. Res.,* **102,** 16 799–16 813.

Lord, S. J., H. E. Willoughby, and J. M. Piotrowicz, 1984: Role of a parameterized ice-phase microphysics in an axisymmetric, nonhydrostatic tropical cyclone model. *J. Atmos. Sci.,* **41,** 2836–2848.

Mango, S. C., and C. W. Lee, 1966: Meteorological classification of natural crystals. *J. Fac. Sci.,* Hokkaido Univ., Ser. 7, 321–362.

Marshall, J. S., and M. K. Palmer, 1948: The distribution of raindrops with size. *J. Meteor.,* **5,** 165–166.

Mason, B. J., 1971: *The Physics of Clouds.* 2d ed. Oxford University Press, 671 pp.

——, 1994: The shape of snow crystals—Fitness for purpose? *Quart. J. Roy. Meteor. Soc.,* **120,** 849–860.

Matrosov, S. Y., 1991: Theoretical study of radar polarization parameters obtained from cirrus clouds. *J. Atmos. Sci.,* **48,** 1062–1070.

——, 1992: Radar reflectivity in snowfall. *IEEE Trans. Geosci. Remote Sens.,* **30,** 454–461.

——, R. F. Reinking, R. A. Kropfli, and B. W. Bartram, 1996: Estimation of ice hydrometeor types and shapes from radar polarization measurements. *J. Atmos. Oceanic Technol.,* **13,** 85–96.

Matson, R. J., and A. W. Huggins, 1980: The direct measurement of the sizes, shapes, and kinematics of falling hailstones. *J. Atmos. Sci.,* **37,** 1107–1125.

May, P. T., A. R. Jameson, T. D. Keenan, P. E. Johnson, and W. Ecklund, 1999a: Combined wind profiler/polarimetric radar studies of the vertical motion and microphysical characteristics of sea breeze thunderstorms. Preprints, *29th Int. Conf. on Radar Meteorology,* Montreal, PQ, Canada, Amer. Meteor. Soc., 347–350.

——, T. D. Keenan, D. S. Zrnić, L. D. Carey, and S. A. Rutledge, 1999b: Polarimetric radar measurements of tropical rain at a 5-cm wavelength. *J. Appl. Meteor.,* **38,** 750–765.

McCormick, G. C., L. E. Allan, and A. Hendry, 1979: The backscatter matrix of ice samples: Its relation to identification of hail by radar. *J. Appl. Meteor.,* **18,** 77–84.

Mead, J. B., P. M. Langlois, P. S. Chang, and R. E. McIntosh, 1991: Polarimetric scattering from natural surfaces at 225 GHz. *IEEE Trans. Antennas Propag.,* **39,** 1405–1411.

Meischner, P. F., V. N. Bringi, M. Hagen, and H. Holler, 1991a: Multiparameter radar characteristics of a melting layer compared with in situ measurements. Preprints, *25th Int. Conf. on Radar Meteorology,* Paris, France, Amer. Meteor. Soc., 721–724.

——, ——, ——, and ——, 1991b: A squall line in southern Germany: Kinematics and precipitation formation as deduced by advanced polarimetric and Doppler radar measurements. *Mon. Wea. Rev.,* **119,** 678–701.

——, C. Collier, A. Illingworth, J. Joss, and W. Randeu, 1997: Advanced weather radar systems in Europe: The COST 75 action. *Bull. Amer. Meteor. Soc.,* **78,** 1411–1430.

Mendel, J., 1995: Fuzzy logic systems for engineering: A tutorial. *Proc. IEEE,* **83,** 345–377.

Metcalf, J. I., A. W. Bishop, R. C. Chanley, T. C. Heitt, and P. J. Petrocchi, 1993: An 11-cm coherent polarimetric radar for meteorological research. *J. Atmos. Oceanic Technol.,* **10,** 249–261.

Mitchell, D. L., 1994: A model predicting the evolution of ice particles, size spectra, and radiative properties of cirrus clouds. Part I: Microphysics. *J. Atmos. Sci.,* **51,** 797–816.

——, R. Zhang, and R. L. Pitter, 1990: Mass-dimensional relationships for ice particles and the influence of riming on snowfall rates. *J. Appl. Meteor.,* **29,** 153–163.

Moninger, W. R., V. N. Bringi, T. R. Detman, J. R. Jordan, T. A. Seliga, and K. Aydin, 1984: Melting layer observations during MAYPOLE. Preprints, *22d Conf. on Radar Meteorology,* Zurich, Switzerland, Amer. Meteor. Soc., 364–369.

Ohtake, T., and T. Henmi, 1970: Radar reflectivity of aggregated snowflakes. Preprints, *14th Radar Meteorology Conf.,* Tucson, AZ, Amer. Meteor. Soc., 209–210.

Pruppacher, H. R., and K. V. Beard, 1970: A wind tunnel investigation of the internal circulation and shape of water drops falling at terminal velocity in air. *Quart. J. Roy. Meteor. Soc.,* **96,** 247–256.

——, and R. L. Pitter, 1971: A semi-empirical determination of the shape of cloud and rain drops. *J. Atmos. Sci.,* **28,** 86–94.

——, and J. D. Klett, 1981: *Microphysics of Clouds and Precipitation.* Reidel, 714 pp.

Rasmussen, R. M., and A. J. Heymsfield, 1987: Melting and shedding of graupel and hail. Part I: Model physics. *J. Atmos. Sci.,* **44,** 2754–2763.

——, V. Levizzani, and H. R. Pruppacher, 1984: A wind tunnel and theoretical study on the melting behavior of atmospheric ice particles: Part III. Experiment and theory for spherical ice particles of radius > 500 μm. *J. Atmos. Sci.,* **41,** 381–388.

Rauber, R. M., K. V. Beard, and B. M. Andrews, 1991: A mechanism for giant raindrop formation in warm, shallow convective clouds. *J. Atmos. Sci.,* **48,** 1791–1797.

Reinking, R. F., S. Y. Matrosov, R. T. Bruintjes, and B. E. Martner, 1997: Identification of hydrometeors with elliptical and linear polarization Ka-band radar. *J. Appl. Meteor.,* **36,** 322–339.

Rosenfeld, D., E. Amitai, and D. B. Wolff, 1995a: Classification of rain regimes by the three-dimensional properties of reflectivity fields. *J. Appl. Meteor.,* **34,** 198–211.

——, ——, and ——, 1995b: Improved accuracy of radar WPMM estimated rainfall upon application of objective classification criteria. *J. Appl. Meteor.,* **34,** 212–223.

Ryzhkov, A. V., and D. S. Zrnić, 1995a: Comparison of dual-polar-

ization radar estimators of rain. *J. Atmos. Oceanic Technol.,* **12,** 249–256.
——, and ——, 1995b: Polarimetric measurements of snow. Preprints, *27th Conf. on Radar Meteorology,* Vail, CO, Amer. Meteor. Soc., 458–460.
——, and ——, 1995c: Precipitation and attenuation measurements at a 10-cm wavelength. *J. Appl. Meteor.,* **34,** 2121–2134.
——, and ——, 1996a: Rain in shallow and deep convection measured with a polarimetric radar. *J. Atmos. Sci.,* **53,** 2989–2995.
——, and ——, 1996b: Assessment of rainfall measurement that uses specific differential phase. *J. Appl. Meteor.,* **35,** 2080–2090.
——, and ——, 1997: Polarimetrically tuned *R*(*Z*) relations and comparisons of radar rainfall methods. *J. Appl. Meteor.,* **36,** 340–349.
——, and ——, 1998a: Discrimination between rain and snow with a polarimetric radar. *J. Appl. Meteor.,* **37,** 1228–1440.
——, and ——, 1998b: Beamwidth effects on the differential phase measurements of rain. *J. Atmos. Oceanic Technol.,* **15,** 624–634.
——, and ——, 1998c: Polarimetric rainfall in the presence of anomalous propagation. *J. Atmos. Oceanic Technol.,* **15,** 1320–1330.
——, ——, and B. A. Gordon, 1998: Polarimetric method for ice water content determination. *J. Appl. Meteor.,* **37,** 125–134.
Sachidananda, M., and D. S. Zrnić, 1985: ZDR measurement considerations for a fast scan capability radar. *Radio Sci.,* **20,** 907–922.
——, and ——, 1986: Differential propagation phase shift and rainfall rate estimation. *Radio Sci.,* **21,** 235–247.
——, and ——, 1987: Rain rate estimates from differential polarization measurements. *J. Atmos. Oceanic Technol.,* **4,** 588–598.
Sassen, K. D., 1987: Ice cloud content from radar reflectivity. *J. Appl. Meteor.,* **26,** 1050–1053.
Schroth, A. C., M. S. Chandra, and P. F. Meischner, 1988: A C-band coherent polarimetric radar for propagation and cloud physics research. *J. Atmos. Oceanic Technol.,* **5,** 803–822.
Sekhon, R. S., and R. C. Srivastava, 1970: Snow size spectra and radar reflectivity. *J. Atmos. Sci.,* **27,** 299–307.
Seliga, T. A., and V. N. Bringi, 1976: Potential use of radar differential reflectivity measurements at orthogonal polarizations for measuring precipitation. *J. Appl. Meteor.,* **15,** 69–76.
——, and ——, 1978: Differential reflectivity and differential phase shift: Applications in radar meteorology. *Radio Sci.,* **13,** 271–275.
Shapiro, A., S. Ellis, and J. Shaw, 1995: Single-Doppler velocity retrievals with Phoenix II data: Clear air and microburst wind retrievals in the planetary boundary layer. *J. Atmos. Sci.,* **52,** 1265–1287.
Smith, P., 1984: Equivalent radar reflectivity factor for snow and ice particles. *J. Climate Appl. Meteor.,* **23,** 1258–1260.
Steinhorn, I., and D. S. Zrnić, 1988: Potential uses of differential propagation phase constant to estimate raindrop and hailstone size distributions. *IEEE Trans. Geosci. Remote Sens.,* **26,** 639–648.
Straka, J. M., 1994: Representing moisture processes in mesoscale numerical models. *Mesoscale Modeling of the Atmosphere, Meteor. Monogr.,* No. 47, Amer. Meteor. Soc., 29–38.
——, 1996: Hydrometeor fields in a supercell storm as deduced from dual-polarization radar. Preprints, *18th Conf. on Severe Local Storms,* San Francisco, CA, Amer. Meteor. Soc., 551–554.
Sun, J., and N. A. Crook, 1996: Comparison of thermodynamic retrieval by the adjoint method with the traditional method. *Mon. Wea. Rev.,* **124,** 308–324.
Takahashi, T., and K. Kuhara, 1993: Precipitation mechanisms of cumulonimbus clouds at Pohnpei, Micronesia. *J. Meteor. Soc. Japan,* **71,** 21–31.
Thomason, J. W. G., A. J. Illingworth, and V. Marecal, 1995: Density and size distribution of aggregating snow particles inferred from coincident aircraft and radar observation. Preprints, *27th Conf. on Radar Meteorology,* Vail, CO, Amer. Meteor. Soc., 127–129.
Tokay, A., and K. V. Beard, 1996: A field study of raindrop oscillations. Part I: Observation of size spectra and evaluation of oscillation causes. *J. Appl. Meteor.,* **35,** 1671–1687.
Tong, H., V. Chandrasekar, K. R. Knupp, and J. Stalker, 1998: Multiparameter radar observations of time evolution of convective storms: Evaluation of water budgets and latent heating rates. *J. Atmos. Oceanic Technol.,* **15,** 1097–1109.
Torlaschi, E., R. G. Humphries, and B. L. Barge, 1984: Circular polarization for precipitation measurement. *Radio Sci.,* **19,** 193–200.
Tuttle, J. D., V. N. Bringi, H. D. Orville, and F. J. Kopp, 1989: Multiparameter radar study of a microburst: Comparisons with model results. *J. Atmos. Sci.,* **46,** 601–620.
Ulbrich, C. W., 1983: Natural variations in the analytical form of the raindrop size distribution. *J. Climate Appl. Meteor.,* **22,** 1764–1775.
——, and D. Atlas, 1982: Hail parameter relations: A comprehensive digest. *J. Appl. Meteor.,* **21,** 22–43.
——, and ——, 1984: Assessment of the contribution of differential polarization to improved rainfall measurements. *Radio Sci.,* **19,** 49–57.
——, and ——, 1998: Rainfall microphysics and radar properties: Analysis methods for drop size spectra. *J. Appl. Meteor.,* **37,** 912–923.
Uyeda, H., R. Shirooka, K. Iwanami, A. Takemoto, and K. Kikuchi, 1991: Observation of vertical structure of convective snow clouds with a dual-polarization radar in Hokkaido, Japan. Preprints, *25th Int. Conf. on Radar Meteor.,* Paris, France, Amer. Meteor. Soc., 717–720.
Vieux, B. E., and P. E. Bedient, 1998: Estimation of rainfall for flood prediction from WSR-88D reflectivity: A case study, 17–18 October 1994. *Wea. Forecasting,* **13,** 407–415.
Vivekanandan, J., and W. M. Adams, 1993: Theoretical investigation of multiparameter radar scattering characteristics of ice crystals. Preprints, *26th Int. Conf. on Radar Meteorology,* Norman, OK, Amer. Meteor. Soc., 109–111.
——, V. N. Bringi, and R. Raghavan, 1990: Multiparameter radar modeling and observations of melting ice. *J. Atmos. Sci.,* **47,** 549–564.
——, R. Raghavan, and V. N. Bringi, 1993a: Polarimetric radar modeling of mixture of precipitation particles. *IEEE Trans. Geosci. Remote Sens.,* **31,** 1017–1030.
——, J. D. Tuttle, and E. A. Brandes, 1993b: Observational and modeling considerations for multiparameter radar detection of hail. Preprints, *26th Int. Conf. on Radar Meteorology,* Norman, OK, Amer. Meteor. Soc., 525–527.
——, V. N. Bringi, M. Hagen, and P. Meischner, 1994: Polarimetric radar studies of atmospheric ice particles. *IEEE Trans. Geosci. Remote Sens.,* **32,** 1–10.
——, D. S. Zrnić, S. M. Ellis, R. Oye, A. V. Ryzhkov, and J. Straka, 1999: Cloud microphysics retrieval using S-band dual-polarization radar measurements. *Bull. Amer. Meteor. Soc.,* **80,** 381–388.
Wakimoto, R. M., and V. N. Bringi, 1988: Dual-polarization observations of microbursts associated with intense convection: The 20 July storm during the MIST project. *Mon. Wea. Rev.,* **116,** 1521–1539.
Waldvogel, A., B. Federer, and P. Grimm, 1979: Criteria for the detection of hail cells. *J. Appl. Meteor.,* **18,** 1521–1525.
Walsh, T. M., 1993: Dual-polarization radar and particle probe measurements in an Oklahoma hailstorm. M.S. thesis, The Pennsylvania State University.
Willis, P. T., 1984: Functional fits to some observed drop size distributions and parameterization of rain. *J. Atmos. Sci.,* **41,** 1648–1661.
Young, K. C., 1993: *Microphysical Processes in Clouds.* Oxford University Press, 427 pp.
Zahrai, A., and D. S. Zrnić, 1993: The 10-cm wavelength polarimetric radar at NOAA's National Severe Storms Laboratory. *J. Atmos. Oceanic Technol.,* **10,** 649–662.
——, and ——, 1997: Implementation of polarimetric capability for

the WSR-88D (NEXRAD) radar. Preprints, *13th Int. Conf. on Interactive Information and Processing Systems for Meteorology, Oceanography, and Hydrology*, Long Beach, CA, Amer. Meteor. Soc., 284–287.

Zrnić, D. S., 1987: Three-body scattering produces precipitation signature of special diagnostic value. *Radio Sci.,* **22,** 76–86.

——, 1991: Complete polarimetric and Doppler measurements with a single receiver radar. *J. Atmos. Oceanic Technol.,* **8,** 159–165.

——, 1996: Weather radar polarimetry—Trends toward operational applications. *Bull. Amer. Meteor. Soc.,* **77,** 1529–1534.

——, and R. J. Doviak, 1989: Effects of drop oscillations on spectral moments and differential reflectivity measurements. *J. Atmos. Oceanic Technol.,* **6,** 532–536.

——, and A. V. Ryzhkov, 1996: Advantages of rain measurements using specific differential phase. *J. Atmos. Oceanic Technol.,* **13,** 454–464.

——, and ——, 1999: Polarimetry for weather surveillance radars. *Bull. Amer. Meteor. Soc.,* **80,** 389–406.

——, N. Balakrishnan, C. L. Ziegler, V. N. Bringi, K. Aydin, and T. Matejka, 1993a: Polarimetric signatures in the stratiform region of a mesoscale convective system. *J. Appl. Meteor.,* **32,** 678–693.

——, V. N. Bringi, K. Aydin, N. Balakrishnan, V. Chandrasekar, and J. Hubbert, 1993b: Polarimetric measurements in a severe hailstorm. *Mon. Wea. Rev.,* **121,** 2221–2238.